RSC
Applied Interfaces

ROYAL SOCIETY OF CHEMISTRY

REVIEW

View Article Online
View Journal | View Issue

Cite this: *RSC Appl. Interfaces*, 2024, 1, 624

Manganese dioxide (MnO_2) and biomass-derived carbon-based electroactive composite materials for supercapacitor applications

Pranoti H. Patil and Sushilkumar A. Jadhav *

Manganese dioxide (MnO_2) is the most promising electrode material for supercapacitors (SCs) due to its low cost, non-toxic nature, high theoretical capacitance, and wide potential window. Meanwhile, biomass-derived carbon has also become a prominent electrode material in recent years due to its cost-effectiveness, eco-friendliness, and availability of biomass in abundance. Carbon can be synthesized from biomass precursors such as plants, animals, and microorganisms *via* various synthesis and activation techniques. MnO_2 is combined with carbon to obtain composite materials with improved electrochemical properties and structural stability. Sustainable porosity in MnO_2-biomass-derived carbon composites increases the conductivity and electrochemical performance of the electrode material. Hence, MnO_2 and biomass-derived composite materials have received great attention regarding their potential use as electrode materials in SCs. Recently, significant new developments in the synthesis and testing of such composite materials have been made. In this review, recent reports about such composite materials are listed and analyzed with numerous examples providing the authors with important collective information. Here, we place a strong emphasis on carbons obtained from a variety of biomass and different types of MnO_2 and composites made from them for SC application. The current challenges and prospects in this field of research are also highlighted.

Received 12th March 2024,
Accepted 2nd May 2024

DOI: 10.1039/d4lf00085d

rsc.li/RSCApplInter

School of Nanoscience and Technology, Shivaji University Kolhapur, Vidyanagar, Kolhapur 416004, Maharashtra, India. E-mail: sushil.unige@gmail.com

1. Introduction

Supercapacitors (SCs) are energy storage devices with unique properties and applications.[1] They are categorized into three

Pranoti H. Patil

Miss. Pranoti Patil obtained her Master of Science degree from Shivaji University Kolhapur, India with an excellent academic record. Her research works are focused on the synthesis and electrochemical testing of biomass-derived carbon, manganese dioxide, conducting polymer and carbonaceous materials such as carbon nanotubes, graphene oxide, and reduced graphene oxide-based binary as well as ternary nanocomposites as electrode materials to be used in supercapacitors and battery type supercapacitors. She is also involved in the synthesis and testing of N-doped graphitic carbon-based composite materials for energy storage applications.

Dr. Sushilkumar A. Jadhav

Dr. Sushilkumar Jadhav obtained his Ph.D. degree from the University of Genova, Italy. He has gained extensive research experience in Europe. At present, he is working as an assistant professor of chemistry in the School of Nanoscience and Technology, Shivaji University, Kolhapur. His research works are focused on the synthesis of various hybrid, porous, and polymer-grafted nanomaterials for energy storage, drug delivery, environmental remediation, and nanocatalysis applications. He is involved in various multidisciplinary research projects. He is also a member of important scientific organizations at national and international levels.

types: electric double-layer capacitors (EDLCs), pseudo capacitors, and hybrid-based devices, each with a different energy storage mechanism.[2] EDLCs use carbon and non-faradaic reactions to store charge. Faradaic reactions are used in pseudocapacitive materials such as metal oxides (MOs), metal sulfides, metal hydroxides, and polymers. Hybrid devices combine the advantages of EDLCs and pseudocapacitive materials to enhance energy density.[3] However, compared to batteries (which have an energy density of 30–200 W h kg^{-1}), SCs have a lower energy density (20 W h kg^{-1}).[4] They need to have a high energy density to be compact. To overcome this problem, a lot of research is being conducted regarding the synthesis and development of novel electrode materials. To enhance the electrochemical properties of SCs, the choice of electrode materials and their fabrication are crucial. SC electrodes must have chemical stability, surface wettability, high thermal stability, high specific surface area, corrosion resistance, and high electrical conductivity. Additionally, they must be affordable and environmentally sustainable.[5–7] In actuality, electrochemical factors are not only influenced by the surface area but also by other crucial parameters such as morphology, including distributions of pore sizes and availability of active sites for the electrolyte.[8–10] The smaller the pore size, the greater the capacitance and the higher the energy density, but it suffers from lower power density. Therefore, the selection of electrode material is critical. Different electrode materials are being investigated for SCs such as MOs or layered double hydroxides (LDHs), MXene, covalent organic frameworks (COFs), *etc.*[11,12] The most extensively investigated strategies are the development of new electrodes from biomass-derived carbon-based materials and nanostructured materials such as hard carbons, dichalcogenides, bio-mass engineered Mn_xO_y nano-scaled oxides like Mn_3O_4, and metal–organic frameworks (MOFs) as high-capacity electrodes with higher surface area, porosity, capacitance, energy density, and power density.[13–15] Biomass-derived carbon-based materials are extensively used as electrode materials for SCs due to the presence of non-metal elements and various functional groups; also their low cost, easy availability, and environmentally friendly nature make them efficient electrode materials for SCs. Various biomass-derived carbon-based electrode materials are shown in Fig. 1. As a precursor, biomass with naturally hierarchical structures could be a viable option for SCs. Recently, heteroatom-doped carbon materials have attracted much attention as another potential electrode material for a variety of electrochemical applications.[16] The synthesis of heteroatom-doped carbon is reasonably simple as merely changing the synthesis conditions can yield it. But every material has its strengths and weaknesses; Mos suffer from poor cyclic stability, while carbon-based materials suffer from low electrical conductivity. Therefore, there is a need to combine both materials to achieve better electrochemical performances.

In comparison to bulk MO materials which have a lower specific area and capacitance, the emerging trend of designing and fabricating innovative porous nanostructure composites with carbon materials is beneficial to increase the specific surface area and achieve good electrochemical properties. MOs demonstrate many oxidation states and participate in faradaic redox reactions that provide high capacitance. On the other hand, activated carbon (AC) exhibits good conductivity with a large surface area and porosity. MO/AC composites have a wide range of applications in energy storage devices.[17]

Nowadays, bimetallic and trimetallic oxides are often utilized as electrode materials due to their high capacitance and electrical conductivity. Trimetallic oxides, compared to single and bimetallic oxides, showed good electrochemical properties. In comparison to single MOs including NiO, MnO_2, SiO_2, Co_3O_4, V_2O_5, CuO, and ZrO_2, bi- or tri-MOs such as $NiCo_2O_4$ delivered high electrical conductivity. Moreover, the doping of Ni enhances the electrical conductivity from 3.1×10^{-5} of (CO_3O_4) to 0.1 to 0.3 S cm^{-1} of ($Ni_xCO_{3-x}O_4$). Novel heterostructure and nanostructured (OD), (1D) and (3D) mixed MOs are typically porous and can offer more active sites for charge transfer and full contact between the active materials and electrolyte results in the enhancement of

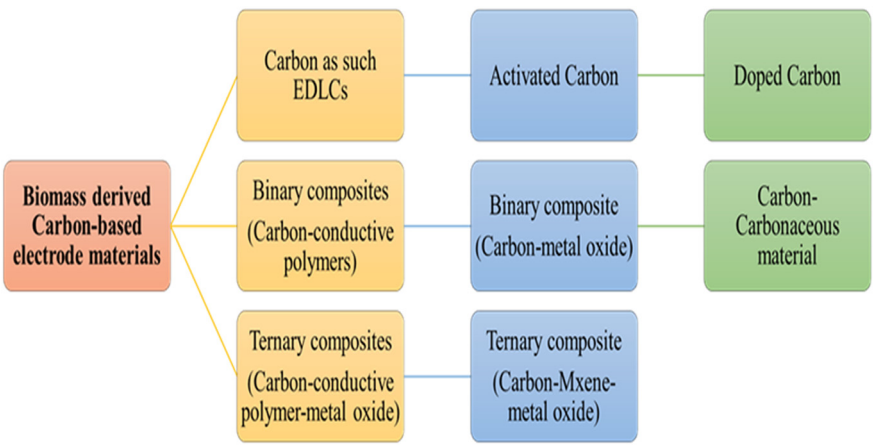

Fig. 1 Biomass-derived carbon-based electrode materials for SCs.

the electrochemical characteristics compared to bulk MO materials. Recently, plant-based AC has attracted much attention due to its natural 3D porous structure, which plays a vital role in the storage and rapid migration of electrolyte ions and can compensate for the underdeveloped pore structure of conventional AC.[18–25] AC made from biomass is abundant in functional groups and non-metal elements like N, S, and O that can be used in faradaic processes to create specific types of pseudo capacitors. When compared to conventional AC, biomass-derived AC is renewable, affordable, and environmentally benign. It is possible to predict that biomass-derived AC will eventually replace conventional AC as the dominant trend in the development of AC. An abundance of porous structures makes AC a good material to make a composite with MnO_2.

The importance of MnO_2 and activated carbon materials has been pointed out separately and the electrochemical and charge storage properties of these materials were investigated in several studies. The main aim of this review is to point out the importance of MnO_2 and biomass-derived carbon-based electroactive composite materials for energy storage application. Herein, we have initially presented the basic and important information about MnO_2 and its various types and their role in energy storage devices. Then the information about biomass-derived carbon is presented by highlighting the characteristic properties of carbons and importance of activation. This section also highlights different biomass sources to produce the carbon. Meanwhile, the main section about the MnO_2-biomass-derived carbon-based composite materials contains discussion of several recent examples of such composites for SC application. The electrochemical properties shown by such composites are correlated to the type, structure, morphology, and shape of MnO_2 and the source of biomass from which the carbon is obtained as well as the main properties of the carbon such as N-doping and porosity. The review is concluded by highlighting the main findings and possible future directions in this field of research.

2. MnO_2: a famous supercapacitive material

Among all transition MOs, MnO_2 is the most promising electrode material because of its various advantages, such as excellent faradaic properties, superior electrochemical performance for pseudo capacitors, high theoretical capacitance (1370 F g^{-1}), and a wide potential window.[26–29] It has higher theoretical capacity than a typical graphite anode and low conductivity which limits the capacitance of thick MnO_2 electrodes.[30] The Mn ion exists in different oxidation states such as +2, +3, +4, +6 and +7. Nanostructured MnO_2 can be synthesized by different methods such as hydrothermal synthesis, solvothermal synthesis, precipitation, thermal decomposition, and sol–gel. MnO_2 has excellent electrochemical properties in neutral electrolytes which guarantees less chemical corrosion of the collector.[31] MnO_2 may get easily dissolved in the electrolyte and this harms its cycling performance. The material's poor electron-transporting capacity also restricts its capacitive efficiency and makes it incapable of exhibiting high-power performance, which limits its potential for use in SCs. MnO_2 has been reported in a variety of nanostructures, including nanosheets, nanorods, nanowires, nanoflakes, nanoflowers, and nanoplates. MnO_2 exhibits a variety of crystalline phases by joining the MnO_6 octahedron unit in various ways, α-, β-, γ-, ε-, δ- and λ-MnO_2 which are shown in Fig. 2.[32] The specific capacitance of these crystalline phases decreases in the order of $\alpha > \delta > \gamma > \lambda > \beta$. It can be divided into three types, including a 1D tunnel structure, 2D layered structure, and 3D mesh structure.[33] The performance of MnO_2 electrode materials is significantly influenced by their polymorphs. Due to the several polymorphs, it exhibits hierarchical electrochemical characteristics. The shape, surface area, and tunnel size of MnO_2 might vary depending on the conditions and synthesis process used. The atom configurations inside these diverse crystallographic phases result in various sorts of pores, which have an effect on the electrolytic ion moment or electron transfer process in the charge storage mechanism.[34] Types of MnO_2 are discussed in detail in the following section.

Types of MnO_2

1) α-MnO_2: Recently, α-MnO_2 has been intensively studied as an electrode material for SC application. α-MnO_2 is a non-toxic, affordable, and environmentally friendly electrode material with a wide potential window.[19] For these reasons, it is a favourable material for electrochemical capacitors.[35] It has a tetragonal crystal system with a Hollandite type of structure with a chain-like 1D tunnel structure (2 × 2) which is made up of shared chains and shared angles.[36] The tunnel size of α-MnO_2 is ~4.6 Å. The majority of cations, including K^+, Li^+, Na^+, Mg^{2+}, Ca^{2+}, and others, can flow *via* this tunnel.[37] Different nanostructured α-MnO_2 electrode materials were studied, including those having nanowire, nanotube, nanorod, nanoneedle, and nanosheet morphologies.[38–40] One-dimensional nanowire structures stand out among them because they have the shortest effective dimension for electron transport and active site exposure, making them important in electrical devices. Due to its crystalline size, shape, chemical composition, and physical characteristics, it exhibits good electrochemical performance.[41,42] Because of the large surface area of α-MnO_2, the capacitance and energy storage capacities are improved. Chettiannan *et al.* fabricated an asymmetric SC using α-MnO_2 nanoflowers on zinc-terephthalate MOFs. The electrode material is synthesized by the conventional solution phase synthesis technique. The synthesized electrode material delivered a specific capacitance of 880.58 F g^{-1} at a current density of 5 A g^{-1} with a 6% loss of capacitance retention after 10 000 cycles. The MnO_2@Zn-MOF composite electrode material exhibited a notably better performance

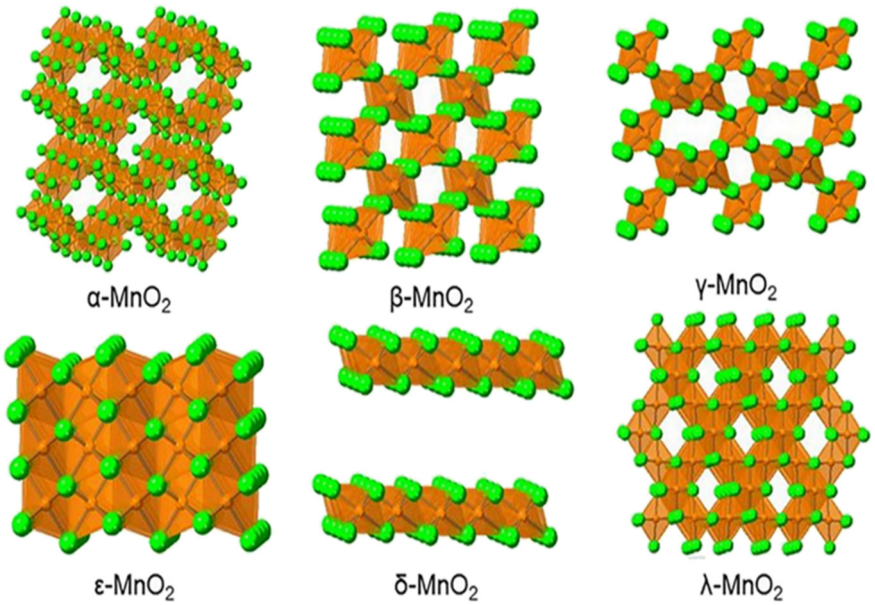

Fig. 2 Schematic diagram of the crystal structure of α-, β-, γ-, ε-, δ- and λ-MnO_2. Reproduced from ref. 32 with permission from RSC, copyright 2022.

due to its unique morphology with enhanced reactive sites and redox-active MnO_2. The asymmetric SC displayed a specific capacitance of 160 F g^{-1} at 3 A g^{-1} with an energy density of 40.68 W h kg^{-1} at a power density of 2024.98 W kg^{-1}. The device also showed a capacitance retention of 90% after 10 000 cycles.[43] Furthermore, Patil *et al.* prepared α-MnO_2 coated with polyaniline (PANI) and reduced graphene oxide (rGO) for SC application. The specific capacitance of the α-MnO_2/PANI composite material was increased by using rGO. The α-MnO_2/PANI/rGO composite displayed a specific capacitance of 261 F g^{-1} at a scan rate of 5 mV s^{-1} with a 25% loss of capacitance retention after 2000 cycles at a current density of 5 A g^{-1}. The composite material exhibited an energy density of 11 W h kg^{-1} at a power density of 1250 W kg^{-1}.[44]

2) β-MnO_2: The tetragonal crystal system of β-MnO_2 has a pyrolusite-like structure. In β-MnO_2, a 1D (1 × 1) tunnel structure is formed. The tunnel has a diameter of 1.89 Å. The central location of the [MnO_6] octahedron is occupied by the Mn atom and the hexagonal space is occupied by the O atom. With this arrangement, a single chain, tightly packed angular structure is created. Only smaller ions, such as H^+ and Li^+, can pass through this tunnel. In terms of thermodynamic stability, β-MnO_2 is a more stable polymorph of MnO_2.[45,46] Pundir *et al.* synthesized 1D β-MnO_2 nanowires for a high-performance SC. The electrode material exhibited a specific capacitance of 213 F g^{-1} at 0.2 A g^{-1} current density with >97.5% capacitance retention after 5000 cycles. In addition, the fabricated symmetric SC showed a specific capacitance of 37.57 F g^{-1} at 0.2 A g^{-1}. It delivered a remarkable capacitance retention of 101.1% after 5000 cycles.[47]

3) γ-MnO_2: The hexagonal crystal system of γ-MnO_2 has a distorted boehmite structure. The structure of γ-MnO_2 is packed hexagonally. Pyrolusite (1 × 1 type) and rhodochrosite (1 × 2 type) develop irregularly in alternation in γ-MnO_2. The interlayer distance is about 1.89 Å.[36] Typically, γ-MnO_2 is used in SCs and batteries because it maintains its stability in an acidic electrolyte. γ-MnO_2 also exhibits good electrochemical performance for pseudocapacitors.[48]

4) ε-MnO_2: ε-MnO_2 is a hexagonal crystal system. In ε-MnO_2, an irregular tunnel structure is formed. Also, it forms a 3D network structure. The majority of the [MnO_6] octahedron gap is distributed by Mn^{4+}.[36]

5) δ-MnO_2: The monoclinic crystal structure of δ-MnO_2 has a birnessite-like structure. The layered structure of δ-MnO_2 contains structural water and non-stoichiometric mixtures of Mn(IV)/Mn(III) or Mn(IV)/Mn(II). It exhibits both EDLC and pseudocapacitive processes as a result of its multilayer structure.[49] To synthesise δ-MnO_2, just the shared edges of the [MnO_6] octahedron are utilised. The shared edges of the [MnO_6] octahedron form its 2D layered structure. The extremely distinctive material δ-MnO_2 quickly changes into various tunnel configurations during synthesis due to its composition of edge-sharing MnO_6 octahedra in a multilayer packing. The tunnel width of δ-MnO_2 is approximately 7 Å. Numerous metal cations, water molecules, and other substances can travel through the tunnel.[45]

6) λ-MnO_2: It is like γ-MnO_2. It has a spinal-like shape. Pyrolusite and rhodochrosite grow irregularly and alternately, producing λ-MnO_2. As a result, λ-MnO_2 takes the shape of a 3D network structure. The potential window reported for λ-MnO_2 is 2 V.[19,45] Some examples of MnO_2 are explained below in the field of energy storage devices such as SCs and batteries.

Discussed below are some representative examples of the use of MnO_2-based materials for SC application.

Jayachandran *et al.* produced α-MnO_2 nanorods as an electrode material for high-quality SCs. In three distinct aqueous electrolytes, including 1 M Na_2SO_4, 0.5 M KOH, and 1 M Na_2SO_4 + 0.5 M KOH, they examined the electrochemical performance of MnO_2 nanorods. In this study, 1 M Na_2SO_4 + 0.5 M KOH showed outstanding electrochemical performance. It produced a 570 F g^{-1} specific capacitance at 1 A g^{-1} current density and 20% capacitance retention loss over 10 000 cycles.[50] Moniruzzaman *et al.* synthesized a cobalt doped@MnO_2 nanosheet composite on highly conductive nickel foam for SC application. The composite material delivered a specific capacitance of 337.8 F g^{-1} in 2 M KOH at 0.5 A g^{-1} current density. This material exhibited a huge loss of capacitance retention *i.e.* 13% for 3000 charge–discharge cycles.[51] Deng *et al.* fabricated α-MnO_2 electrodes for high-performance asymmetric sodium (Na) ion SCs. In this work, they introduced a pre-activation strategy into the α-MnO_2 nanosheet electrode to enhance the Na-storage performance. Based on α-MnO_2 positive and m-WO_3 negative, they developed a novel aqueous ASSC in aqueous Na_2SO_4 electrolyte. The electrode material showed a volumetric capacitance of 377 F cm^{-3} with an excellent capacitance retention of 123% after 10 000 cycles. It delivered an energy and power density of 0.965 W h cm^{-3} and 65.2 W cm^{-3} respectively.[52] Dai *et al.* reported the effect of current density on the electrochemical performance of MnO_2 electrodes of SCs and lithium-ion batteries. In SCs, the electrode material showed a specific capacitance of 415.4 F g^{-1} at the current density of 1 A g^{-1} while in a lithium-ion battery, it delivered 818. 1 mA h g^{-1} at 1 A g^{-1} after 200 cycles. The MnO_2 electrode exhibited an energy density of 1000 mA g^{-1} in a lithium-ion battery.[53] For high-performance aqueous SCs, Wu *et al.* prepared zinc (Zn)-doped MnO_2 ultrathin nanosheets with defects. The Zn ion doped in MnO_2 results in an increase of conductivity of the electrode material. The prepared material showed a specific capacitance of 392 F g^{-1} with a good capacitance retention of 95.2% after 10 000 cycles. It delivered an energy density of 55.28 W h kg^{-1} at a power density of 555.6 W kg^{-1}.[54] Saini *et al.* fabricated an asymmetric device using $ZnCo_2O_4$@MnO_2 with a porous nanosphere decorated flower-shaped structure. The asymmetric device delivered a specific capacitance of 791.11 F g^{-1} at a 5 A g^{-1} scan rate with an energy density of 247.22 W h kg^{-1} at a power density of 1250 W kg^{-1}. $ZnCo_2O$@MnO_2 showed a significant specific capacitance of 4223 F g^{-1} in 6 M KOH in 1 A g^{-1}. It exhibited only a 3% loss of capacitance retention after 5000 cycles.[55]

3. Biomass-derived carbon

Carbon plays an important role in energy storage devices. Coal, natural gas, and biomass are all sources of carbon-based materials but biomass is a renewable and natural source of carbon. The surface area and tunable porous architecture of biomass-derived carbon make it an efficient electrode material in the field of energy storage devices. Additionally, due to its natural abundance, low cost, non-toxicity, environmental friendliness, and biocompatibility, it is frequently used by researchers as a promising electrode material for SCs.[56] It is synthesized from naturally present biomass precursors such as wood, agricultural waste, and other organic materials. Additionally, plant-based biomaterials (such as sugar cane bagasse, orange peel, soybean, aquatic weeds, banana peel, peas, and maize cob) as well as animals and microorganism-based biomass (such as fungal [mushroom] and bacterial cellulose) have been established. While choosing a carbon source from biomass, the precursor should have a significant number of cross-linked molecules, a low elemental oxygen content, a high molecular weight, and thermally stable molecules. It exists in different morphologies, including 0D spherical, 1D fibrous, 2D sheet, and 3D porous structure.[57] The carbon compounds prepared from biomass can be used in various reactions, including electrocatalytic, photocatalytic, and organic transformations.[58–60] Biomass-derived carbon materials are synthesized by processes like pyrolysis and thermal carbonization. Pyrolysis is a dry-carbonization reaction that takes place at high temperatures (between 300 °C and 900 °C) in an inert atmosphere or low-oxygen environment. In pyrolysis, the performance of carbon is influenced by the catalyst, temperature, and time. On the other hand, thermal carbonization is a chemical process that transforms biomass into carbonaceous compounds and takes place in an aqueous environment at a higher temperature (300 °C) and high self-generated pressure. In this process, the water-to-biomass ratio, temperature, pressure, and duration are crucial. In comparison to pyrolysis, thermal carbonization produces more biochar yield.[61] It can also be obtained by physical and chemical activation methods. Physical activation is carried out in the presence of air, steam, or gas. At low temperatures (<500 °C), air activation is carried out. Steam is the most favorable activating agent that is conducted at 800–1200 °C. The activation of CO_2 is conducted at a higher degree of graphitization. Chemical activation is carried out at 450–900 °C in the presence of KOH, NaOH, $ZnCl_2$, $FeCl_3$ or H_3PO_4.[62]

Biomass-derived carbon has several notable features such as high carbon content, porosity, and stability. Compared to conventional carbon materials, it has a larger charge storage capacity, faster charge/discharge rates, and longer cycle life due to its wide surface area. It can resist high temperatures without degrading because of its relatively good thermal stability.[63] Pore size distribution, connectivity, and wettability of porous carbon are significant characteristics that have an impact on the ion diffusion and energy density of active materials. The entry of ions into pore systems and the transport of electrons are significantly influenced by the wettability of the pores. There are many different kinds of porous carbon materials, including microporous, mesoporous, and microporous, each of which has a specific function in the ion storage and transport kinetics of the material.[64] Macro pores serve as ion reservoirs. They can store a large quantity of ions and act as a buffer or storage

area. It keeps the ion concentration stable within the material. Furthermore, mesoporous materials are small to medium-sized porous carbon materials that offer several channels for ions to permeate through a substance. They provide ion transport by promoting ion movement within the porous carbon. This helps to maintain even ion distribution throughout the material. Materials with microporosity can present a challenge for ions due to their size. Even though some micropore regions might not directly absorb ions, they still have an impact on the material's overall charge condition. The overall charge storage capability of the porous carbon material may be impacted by the selective ion diffusion. For the structure of porous carbon, interconnected pores of various sizes are essential. The creation of 3D interconnected microporous and mesoporous structures is still challenging. To achieve acceptable wettability, surface modification of porous carbon materials is progressively becoming an issue. The majority of biomass contains heteroatoms, which increase the number of active sites and decrease the hydrophobicity of porous carbon. These components include boron, nitrogen, sulfur, and other trace elements.[61] Hence, biomass-derived carbon materials are considered as the most promising electrode materials for energy storage devices. Recently reported examples of biomass-derived carbon as electrode materials for energy storage devices such as batteries and SCs are discussed below.

Mariappan *et al.* constructed a MnFe layer double hydroxide on carbon derived from orange peel for electrocatalytic water splitting. The MnFe-biomass-derived carbon catalyst was synthesized by pyrolysis followed by the hydrothermal method. The electrocatalyst showed better hydrogen evolution reaction and oxygen evolution reaction activities in 1 M KOH. Due to the synergic effect between MnFe-LDH and carbon, it achieved noteworthy electrolytic performance.[65] Sui *et al.* synthesized biomass-derived carbon-coated SiO_2 nanotubes for lithium-ion batteries. They used SiO_2 nanotubes (SNTs) as an effective anode material due to their excellent properties and lignin furfural resin (C-PDLF) derived carbon as a cathode material for lithium-ion batteries. SNTs@C-PDLF exhibited 661 mA h g^{-1} specific capacity at 100 mA g^{-1}. Compared with pristine SNTs, SNTs@C-lignin showed a better life span.[66] For hydrogen fuel cells, Ding *et al.* prepared carbon derived from brinjal peel immobilized ultrafine Pt nanoparticles as a highly efficient catalyst. The prepared catalyst exhibited a power density of 1.246 V cm^{-2} at 2000 mA cm^{-2} in an H_2 air fuel cell.[67] Jin *et al.* constructed biomass carbon quantum dots from a spent coffee ground modified TiO_2 photocatalyst for methylene blue degradation. The TiO_2 catalyst showed high photocatalytic activity as well as chemical stability. N-doped carbon quantum dots (NCQDs) were used to decorate TiO_2. As compared to pristine TiO_2, 3-NCQDs/TiO_2 showed a faster degradation rate for methylene blue. It also showed an adequate photocatalytic degradation rate of 93.1% within 60 min.[68] Wang *et al.* synthesized N, P co-doped hard carbon derived from tea tormenta material for Na-ion batteries. The material showed excellent electrochemical performance due to the active sites in N and P groups.[69] Zhang *et al.* synthesized a Cu-doped bamboo/polypyrrole-derived porous carbon material for SCs. Moreover, they used citric acid and copper sulfate as catalysts. Due to the synergic effects of catalysts and heteroatom doping the synthesized composite material exhibited good electrochemical performance. It showed the lowest energy density of 17.42 W h kg^{-1} at the highest power density of 5000 W kg^{-1} in Na_2SO_4 aqueous electrolyte.[70] For high-performance SCs, Wang *et al.* synthesized hierarchical cornstalk-derived porous carbon (CSPC) with decorated Ag-nanoparticles. The materials were characterized using SEM and TEM as shown in Fig. 3. The CSPC-Ag electrode has a higher specific capacitance because it uses electron transport channels and active sites of Ag NPs to facilitate electrolyte ion diffusion.[71]

Yao *et al.* synthesized cheese-like hierarchical porous red dates derived activated carbon (RDAC) materials for high-performance SCs. Furthermore, Fig. 4 illustrates the SEM images of RDAC-0 and RDAC-4 samples. The material exhibited a large specific surface area (SSA) of 1115.7 m^2 g^{-1}. Due to the large SSA and porous structure, the material showed good electrochemical properties.[72]

Agrawal *et al.* fabricated a symmetric SC using waste biomass *Phyllanthus emblica* leaves (PELC) derived high-performance AC (PELAC). The surface characterizations are depicted in Fig. 5. The PELAC electrode exhibited good cyclic stability *i.e.* 98.7% capacitance retention after 8000 cycles at 10 A g^{-1} in KOH electrolyte. The symmetric SC showed an energy density of 29 W h kg^{-1} at a remarkable power density of 6750 W kg^{-1} in PVA/KOH.[73]

Mehdi *et al.* prepared biomass-derived carbon from date seeds for SC application. The date seed biochar (DSBC) material was synthesized by slow pyrolysis at 600 °C (DSBC-600) and chemical activation at 700 °C (DSAC-700), 800 °C (DSAC-800) and 900 °C (DSAC-900) by H_2SO_4. Fig. 6 shows SEM images at different temperatures. Due to 3D porous structure, DSAC-700 showed good specific capacitance of 487.5 F g^{-1} at 1 A g^{-1}.[74]

For a high mass loading SC, Tian *et al.* synthesized porous carbon from *Linum usitatissimum* L. root by a facile *in situ* activation method. The material was carbonized at 800 °C for 1 h in a N_2 atmosphere. The synthesized material enhanced surface utilization and ion diffusion due to active sites as shown in Fig. 7. The material showed gravimetric/volumetric/areal capacitances of 421 F g^{-1} /316 F cm^{-3} /8.0 F cm^{-2} at 1 A g^{-1}. The symmetric SC delivered an energy density of 8.16 W h kg^{-1}.[75]

Li *et al.* prepared N, P co-doped hierarchical porous carbon nanosheets derived from pomelo peel for SC application. The co-doping improved the conductivity, morphology, and specific surface area of the material. Fig. 8 shows the SEM images of the synthesized material. At 750 °C temperature, the N, P co-doped material exhibited an energy density of 36 ± 1.5 W h kg^{-1} and power density of 1000 W

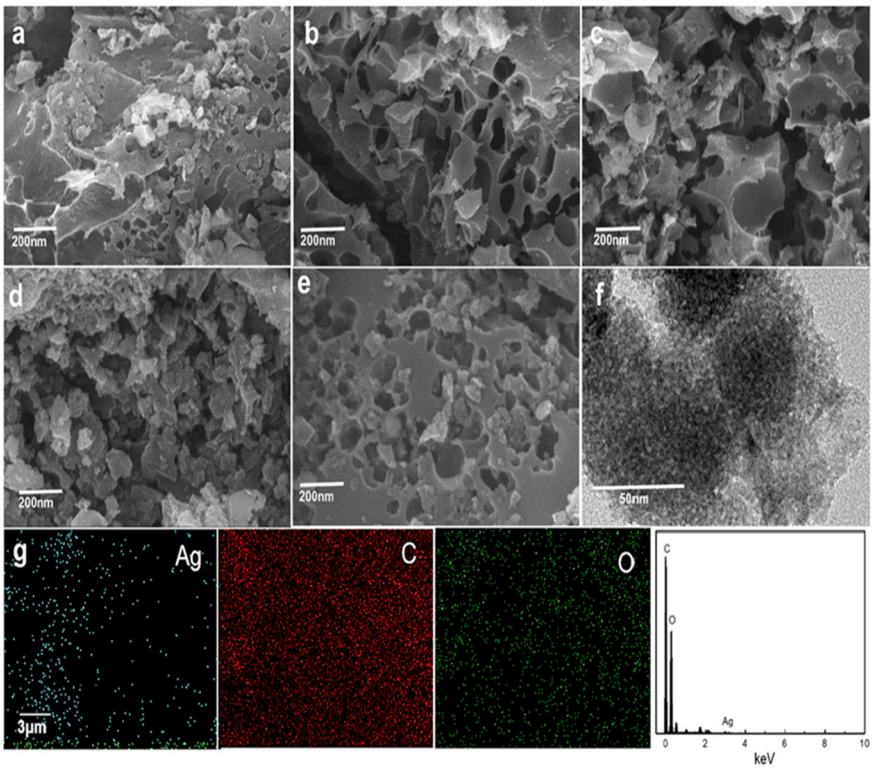

Fig. 3 SEM images of CSPC-0.5 (a), CSPC-1 (b), CSPC-1.5 (c), CSPC-2 (d) and CSPC-1-5% Ag (e); (f) TEM image of CSPC-1-5% Ag; (g) EDS element mapping analyses and spectrum of CSPC-1-5% Ag. Reproduced from ref. 71 with permission from Elsevier, copyright 2022.

kg^{-1}. It also showed outstanding capacitance retention of 99% after 10 000 cycles.[76]

Tarimo *et al.* fabricated a symmetric SC device from a waste chicken bone-derived carbon electrode material. The SEM and TEM images at different magnifications are shown in Fig. 9. The material was carbonized at 700 °C for 2 h under an Ar atmosphere. Due to carbonization, the material

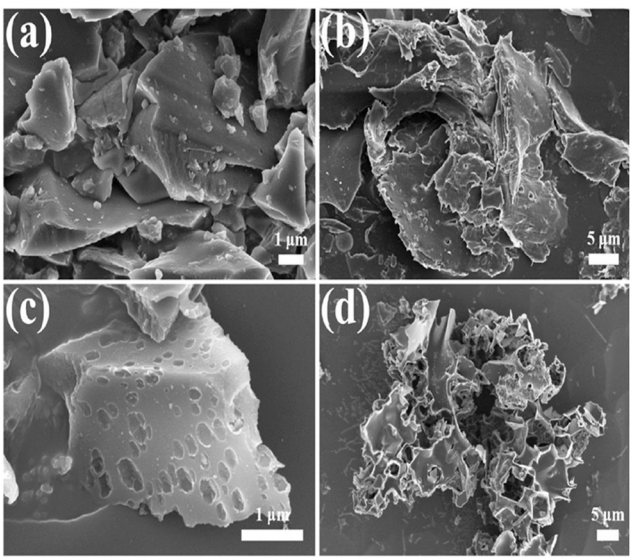

Fig. 4 SEM images of the samples: (a and b) RDAC-0-800; (c and d) RDKC-4-800. Reproduced from ref. 72 with permission from Elsevier, copyright 2023.

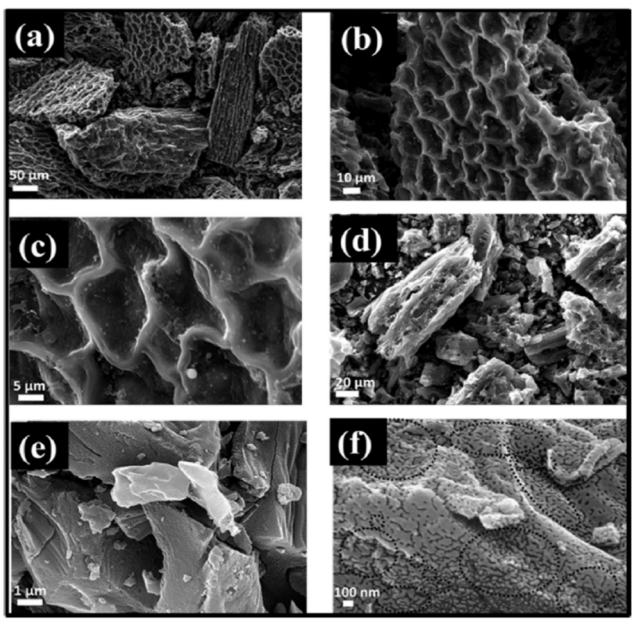

Fig. 5 (a–c) SEM images of PELC-800, (d) SEM image of PELAC, and (e and f) FESEM images at different magnifications (inset dotted circles indicate many tiny pores/surface defects existing inside the material at the 100 nm scale). Reproduced from ref. 73 with permission from Elsevier, copyright 2023.

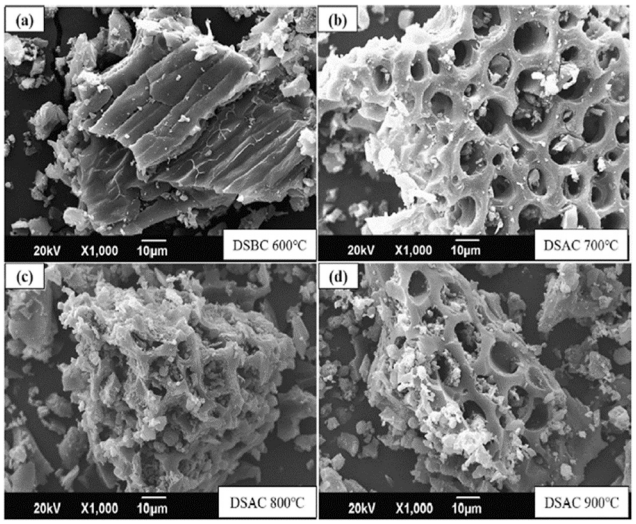

Fig. 6 (a) SEM micrographs for biochar produced at 600, (b) shows a micrograph of DSAC700, (c) shows a micrograph of DSAC800, and (d) shows a micrograph of DSAC900. Reproduced from ref. 74 with permission from Elsevier, copyright 2023.

improved pore size and specific surface area (2235.8 $m^2 g^{-1}$).[77]

Overall, the synthesis of biomass-derived carbon materials as electrodes is a subject of intense research. Recently used biomasses obtained from various biomass-derived carbon precursors, their synthesis methods, and conditions with dimensions, porosity, and surface area are listed in Table 1.

4. MnO_2-Biomass-derived carbon-based composites

In comparison to pure MOs, the combination of MO with carbon-based nanostructures has demonstrated superior

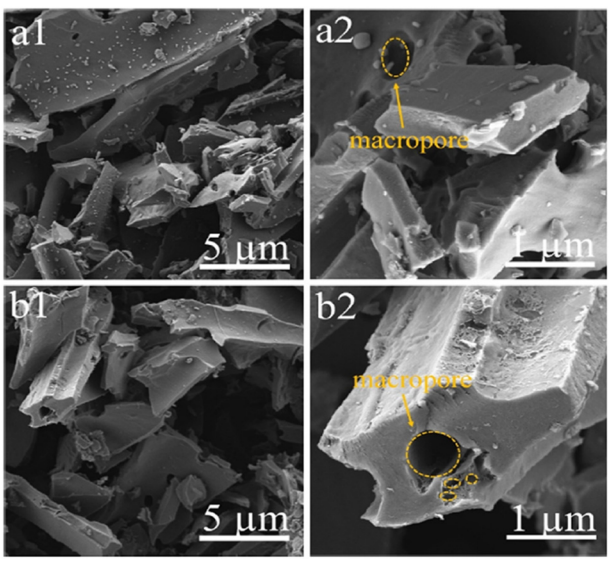

Fig. 7 SEM images of LRC-0 (a1 and a2) and LRC-1 (b1 and b2). Reproduced from ref. 75 with permission from Elsevier, copyright 2023.

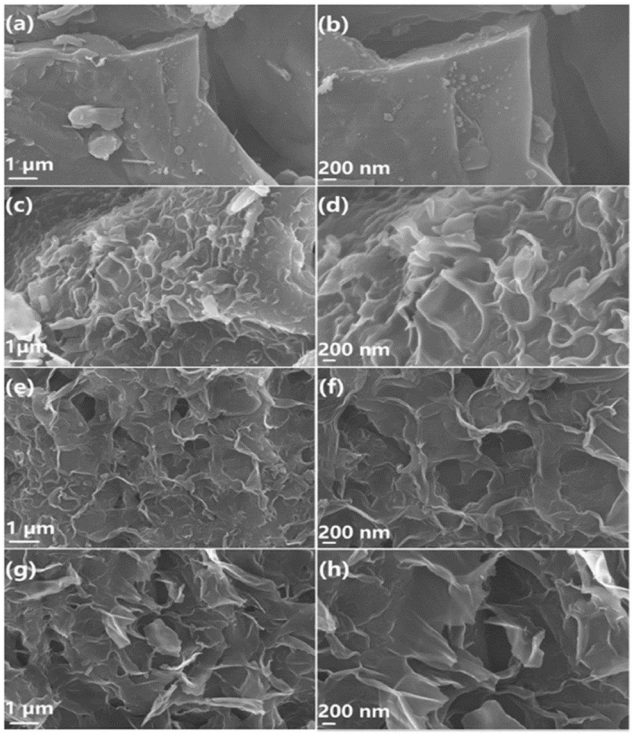

Fig. 8 SEM images of (a and b) BC, (c and d) NPCNs-650, (e and f) NPCNs-750, and (g and h) NPCNs-850. Reproduced from ref. 76 with permission from Elsevier, copyright 2022.

performance in galvanostatic cycling investigations.[103] Recently, MO–carbon composites have attracted considerable attention because of their chemical, physical, electrical, and optical properties as well as many potential applications.[104,105] The composite combines the energy characteristics of pseudocapacitive materials (*via* fast redox reversible reaction) with cyclic stability and power characteristics of carbon materials (electrostatic fast ion adsorption and desorption at electrode–electrolyte interfaces) and boost cycle life. The composite materials have various benefits over conventional electrode materials. Due to more active sites for transporting electrolyte ions and a wider potential window, the composite results in high specific capacitance, good stability, and high energy and power densities.[106] MnO_2 is a low-cost, non-toxic and environmentally friendly MO. Additionally, it has strong electrochemical functionality for energy storage systems. Its high specific capacity but its poor conductivity and stability limits its application as an SC.[107] Biomass-derived carbon can improve the electrical conductivity of MnO_2 by forming a conductive network or coating on the surface of MnO_2. This can increase the charge transfer rate and reduce the internal resistance of the electrode.[108] A comparatively large surface area, high stability, superior electrical conductivity, and cost-effectiveness all are the features of porous carbon's structure. Porous carbon has been widely employed in batteries and SCs because of its tremendous benefits.[109] MnO_2 easily collapses therefore, carbon combines with it to give structural

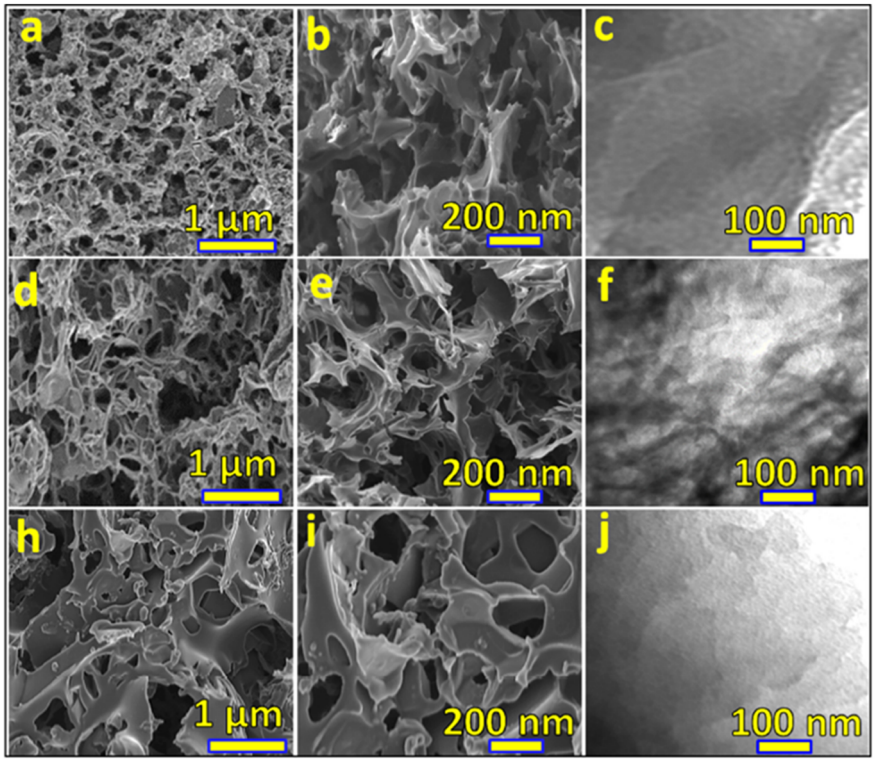

Fig. 9 (a and b), (d and e) and (h and i) are SEM images of CCBW-0.5, CCBW-1, and CCBW-2 at low and high magnifications, respectively. (c), (f) and (j) are TEM images of CCBW-0.5, CCBW-1, and CCBW-2, respectively. Reproduced from ref. 77 with permission from Elsevier, copyright 2022.

stability. MnO_2 and biomass-derived carbon composites have high energy densities, good rate capabilities, and extended cycle life, making them suitable electrode materials for SCs.[110] However, there are still some challenges and opportunities for further improvements, such as optimizing the synthesis methods, enhancing the conductivity and stability of the composites, exploring new biomass sources, and designing novel architectures.

MnO_2 and N-doped biomass-derived carbon

N-doping improves carbon materials' capacitance and conductivity by introducing pseudo-capacitance and active sites.[111–113] In N-doped carbons, the nitrogen functional groups are typically found in the molecular configurations (chemical states) (Fig. 10): quaternary nitrogen is referred to as "graphitic nitrogen" or "substituted nitrogen", in which nitrogen atoms are integrated into the carbon network. Pyridinic nitrogen refers to nitrogen atoms at the edges of graphite planes, each of which is bonded to two carbon atoms and donates one π electron to the aromatic system; pyrrolic N refers to nitrogen atoms that are bonded to two carbon atoms and contributes two π electrons to the system.[114]

MnO_2/N-doped biomass-derived carbon composites have been synthesized using various techniques, including solution growth, hydrothermal treatment, vapor deposition, *etc.* Compared to pure MnO_2 or carbon materials, the composites have better chemical performance and stability for SCs.[115–117] For examples, one study reported that MnO_2/N-doped porous carbon spheres prepared from Na alginate showed a specific capacitance of 419.3 F g^{-1} at 1 A g^{-1} and an ultrafast charge–discharge rate of 2.5 V s^{-1}.[118]

Li *et al.* fabricated a quasi-solid asymmetric SC using MnO_2-coated and N-doped pine cone porous carbon (N-PC). MnO_2-coated and N-doped porous carbon was prepared by a carbonization and hydrothermal process. Due to carbonization, the material enhanced the contact area and improved the electron transmission. The asymmetric SC showed a specific capacitance of 167.8 F g^{-1} at 1 A g^{-1} current density with a 15.5% loss of capacitance retention after 3000 cycles in PVA/Na_2SO_4 quasi-solid electrolyte. It also displayed an energy density and power density of 20.42 W h kg^{-1} and 799.9 W kg^{-1} respectively.[119]

Sui *et al.* prepared an asymmetric SC using polypyrrole, MnO_2, and N-doped carbon nanowires (PCNW). The PCNW porous structure made of polypyrrole nanowires serves as a supportive substrate for the deposition of MnO_2 *via* a redox reaction between carbon and $KMnO_4$. The asymmetric SC displayed a specific capacitance of 55.7 F g^{-1} at 0.5 A g^{-1} with an energy density of 23.7 W h kg^{-1} at a good power density of 2000 W kg^{-1}. It exhibited capacitance retention of 87.6% after 10 000 cycles.[120]

For flexible solid-state asymmetric SC, Sun *et al.* synthesized a MnO_2@N-doped AC (NAC) composite. The

Table 1 Conditions, dimensions, pore size, and surface area of various biomass-derived carbon

Sr. no.	Biomass source	Condition of carbonization/pyrolysis under N_2 or in air	Carbon dimensions/pore size/ surface area (m^2 g^{-1})	Ref.
1.	Agaric	Pyrolyzed at 750 °C for 2 h under N_2 atmosphere	— Microporous 2225.5	78
2.	Lignin	Carbonization at 1000 °C for 1 h under N_2 atmosphere	1D Mesopores 674	79
3.	Bamboo	Carbonization at 800 °C for 2 h under N_2 atmosphere	1D Micropores 1987.76	80
4.	Lotus seedpod	Carbonization at 800 °C for 3 h under Ar atmosphere	— Micropores 908.9	81
5.	Marine biowaste	Carbonization at 1000 °C for 1 h under N_2 atmosphere	— Micropores 1526	82
6.	Orange peel	Carbonization at 400 °C for 8 h in air	3D — —	83
7.	*Agave sisalana*	Carbonization at 550 °C for 60 min under N_2 atmosphere	— Micropores and mesopores 1464	84
8.	Oil palm empty fruit bunch	Carbonization at 800 °C for 2 h under N_2 atmosphere	— Mesopores 640.61	85
9.	Palmyra palm flower	Carbonization at 400 °C for 1 h under N_2 atmosphere	— Micropores 950	86
10.	Eggfruit	Carbonization at 500 °C for 4 h under N_2 atmosphere	3D Mesoporous 87.88	87
11.	Acacia wood	Carbonization at 800 °C for 2 h under N_2 atmosphere	3D Nanoporous 1563.43	88
12.	*Cassia fistula* dry fruits	Carbonization at 800 °C for 3 h under N_2 atmosphere	— Mesoporous 625	89
13.	Wood/sticks	Carbonization at 800 °C for 4 h under N_2 atmosphere	3D Microporous and mesoporous 973	90
14.	*Caesalpinia sappan*	Pyrolysis at 800 °C for 1 h under N_2 atmosphere	— Super microporous 675	91
15.	Bamboo	Carbonization at 600 °C for 2 h under N_2 atmosphere	— Micro-mesoporous 1985	92
16.	*Acacia auriculiformis* bark	Carbonization at 800 °C for 2 h under Ar atmosphere	3D Microporous and mesoporous 1147	93
17.	Sugar beet pulp	Pyrolyzed at 700 °C for 150 min in an inert atmosphere	— Micro/mesoporous 950.31	94
18.	Eucalyptus oil	Carbonization at 700 °C for 1 h under N_2 atmosphere	— Microporous 329.66	95
19.	Lemongrass	Pyrolyzed at 600 °C under N_2 atmosphere	— Micro-mesoporous 1694	96
20.	Chicken feet (collagen)	Carbonization at 800 °C for 30 min under Ar atmosphere	3D Microporous 1087	97
21.	Soybean pods	Pyrolyzed at 600 °C for 90 min under Ar atmosphere	3D Mesoporous 1807.56	98
22.	Tobacco waste	Carbonization at 850 °C for 30 min under Ar atmosphere	— Microporous 1079.2	99
23.	Bamboo fiber	Pyrolyzed at 800 °C for 2 h under Ar atmosphere	— Microporous 1900	100
24.	Vegetable sponge	Carbonization at 600 °C for 2 h under N_2 atmosphere	— Mesoporous 1619.3	101
25.	*Pisum sativum*	Carbonization at 800 °C for 2 h under N_2 atmosphere	— Microporous 240	102

N-doped carbon was activated by KOH while the MnO_2@NAC composite was obtained by a simple hydrothermal method. The NAC has significant interactions with MnO_2 due to interface modification, allowing for fast charge transfer. The electrode material showed a specific capacitance of 408.5 F g^{-1} at 0.5 A g^{-1}. The flexible solid-state asymmetric SC fabricated with NAC as the anode and MnO_2@NAC as the cathode in PVA-KOH electrolyte displayed a specific capacitance of 75 F g^{-1} at 1 A g^{-1} current density with 89.5% capacitance retention after 10 000 cycles. It also delivered an energy density of 26.7 W h kg^{-1} at a power density of 400 W kg^{-1}.[121]

Kongthong *et al.* prepared coin- and pouch-cell SCs using N-doped pineapple leaf fiber-derived activated carbon (PALF-NAC) with MnO_2. The α-MnO_2/PALF-NAC electrode material showed a specific capacitance of 195 F g^{-1} at 0.1 A g^{-1} in 1 M H_2SO_4. This electrode material showed good electrochemical performance in coin- and pouch-cell SCs. The specific capacitance exhibited 133 F g^{-1} and 120 F g^{-1} in coin- and pouch-cell SC respectively. In the coin-cell SC, the energy

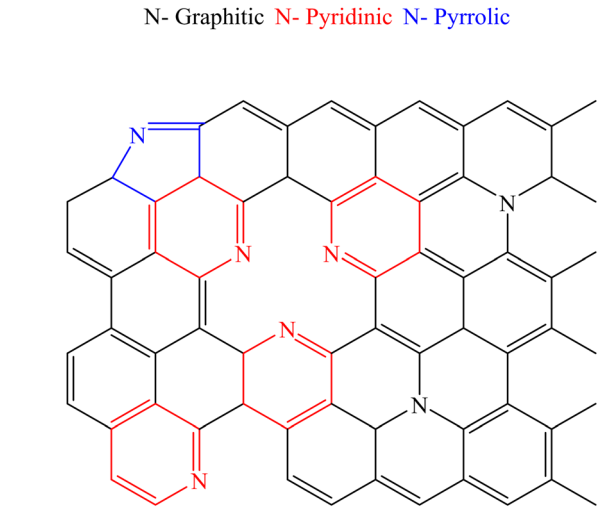

Fig. 10 Molecular structures of N-doped carbon atoms.

density is 27 W h kg^{-1} at 148 W kg^{-1} power density with a capacitance retention of 84% after 10 000 cycles. Similarly in the pouch-cell SC, this electrode material delivered an energy density of 26.8 W h kg^{-1} at a power density of 120 W kg^{-1}.[122]

Li *et al.* fabricated an asymmetric SC using MnO_2 nanosheets and N-doped agaric-derived porous carbon (N-APC). The three-dimensional pore structure of N-APC enhanced the electron transmission. The electrode material exhibited a specific capacitance of 330 F g^{-1} at 1 A g^{-1}. An asymmetric SC developed with N-APC as a negative electrode and MnO_2@N-APC as a positive electrode in 1 M Na_2SO_4 showed an energy density and power density of 28 W h kg^{-1} and 560 W kg^{-1} respectively.[123]

Wang *et al.* reported the multicore–shell MnO_2@Ppy@N-doped porous carbon nanofiber ternary composite electrode material for a high-performance SC. The composite material showed a specific capacitance of 595.77 F g^{-1} with a 4% loss of capacitance retention after 1000 cycles. The asymmetric SC delivered an energy density of 9.36 W h kg^{-1} at 1000 W kg^{-1} power density.[124]

Synergic effects

The MO present in the carbon matrix provides electrical conductivity to the electrons produced during the redox reaction from the MO. It is believed that the device will have outstanding electrochemical performance due to the faradaic redox reaction in MO and the huge specific surface area of AC.[125] The electrical conductivity, specific capacitance, rate capability, and cyclic stability of the electrodes can all be enhanced by the synthesis of a composite of MnO_2 and carbon produced from biomass. The synthesis techniques, shape, and crystal structure of the composite all affect the synergistic effects of MnO_2 and carbon produced from biomass.[126] Layered MnO_2 can limit volume expansion and improve the utilization of MnO_2 such as α-, β-, γ-, ε-, δ-, and λ which have distinct electrochemical features and affinity with carbon materials.[127] Porous carbon can provide more active sites and channels for ion transport inside the film. Therefore, it is essential to optimize the synthesis and production of MnO_2 and carbon composites obtained from biomass to produce high-performance SCs. MnO_2 can be synthesized in different morphologies/shapes such as nanosheets, nanorods, nanoflowers, nano wrinkles, and nanoparticles. There are several reports available regarding MnO_2 nanosheets like morphology and biomass-derived carbon for SC applications. All the experiments except MnO_2/egg yolk by Feng *et al.* were carried out using a three-electrode cell configuration in Na_2SO_4 electrolyte. Some examples are explained below.

Nanosheets

He *et al.* fabricated flax textile-derived carbon fiber cloth coated with MnO_2 nanosheets for SC application. Although flax textile has good stability it suffers from low specific capacitance; therefore to achieve good specific capacitance it is coated with MnO_2 nanosheets. The composite material delivered the highest specific capacitance of 683.73 F g^{-1} at a current density of 2 A g^{-1} and 94% capacitance retention after 1000 cycles. The electrode material showed an energy density of 46.54 W h kg^{-1} at the highest power density of 45.50 kW kg^{-1}.[128]

Li *et al.* prepared a 3D hollow carbon skeleton from lotus pollen and hexagonal MnO_2 nanosheet composite for a high-performance SC. Due to chemical activation in the presence of $KMnO_4$, the MnO_2/C material improved the morphology and enhanced the electrochemical performance. The composite exhibited a high specific capacitance of 257 F g^{-1} at a current density of 0.5 A g^{-1}. It showed an energy density and power density of 51.5 W h kg^{-1} and 303 W kg^{-1} respectively. The composite displayed very high capacitance loss *i.e.* 12% for 2000 cycles.[129]

Mao *et al.* synthesized the fungal conidium-derived carbon/MnO_2 composite for SC application. Sulfur element from conidium enhanced electron transit and created readily available active sites for MnO_2 nanosheet binding. The specific capacitance of 263.5 F g^{-1} was reported at 1 A g^{-1}. The composite material revealed an energy density of 542 W h kg^{-1} at an outstanding power density of 1000 W kg^{-1} but 17% capacitance loss was observed for only 2000 cycles.[130]

The MnO_2/allium-giganteum-like biocarbon (KWB) derived from sugarcane bagasse composite was fabricated by Chen *et al.* KWBM was created by binding MnO_2 nanosheets on the surface of biocarbon. The composite material showed a specific capacitance of 402 F g^{-1} at 1 A g^{-1} in a three-electrode assembly. KWBM-4 was used as the positive electrode and KWB as the negative electrode to create an asymmetric two-electrode setup which exhibited an energy density of 25.9 W h kg^{-1} at a superior power density of 750 W kg^{-1}. The composite material displayed excellent cyclic stability with 94.2% capacitance retention after 2000 cycles.[131]

Chen *et al.* synthesized carbon derived from soybean stalk with MnO_2. They reported that nanostructured MnO_2 with a highly porous and conductive matrix had improved pseudocapacitive kinetics. The electrode material exhibited a specific capacitance of 384.9 F g^{-1} at low current density. It revealed an energy density and good power density of 32.3 W h kg^{-1} and 9.58 kW kg^{-1} respectively. The material showed 90.7% capacitance retention after 5000 cycles.[132]

For a high-performance SC, Kong *et al.* fabricated carbon derived from wheat bran which was further decorated with MnO_2 nanosheets. Due to hierarchical porous carbon, the material enhances ion or electron transmission. MnO_2@PAC as the positive electrode and PAC as the negative electrode were used for the asymmetric SC. The electrode material displayed a specific capacitance of 258 F g^{-1} at 1 A g^{-1}. Also, it exhibited an energy density of 32.6 W h kg^{-1} at a power density of 450 W kg^{-1}. The capacitance retention of 93.6% was achieved after 10 000 charge–discharge cycles.[133]

Feng *et al.* reported biomass-derived carbon with incorporation of MnO_2 for SC application. In this work, P, N, and O-tri-doped egg yolk-derived carbon were used. The heteroatom-doped biomass-derived carbon improved electrochemical properties. The electrode material delivered a specific capacitance of 341 F g^{-1} at a current density of 1 A g^{-1}. The electrode material exhibited a power density of 0.2 W kg^{-1} with 38.4 W h kg^{-1} energy density and low capacitance loss was observed for 10 000 cycles. In this report, the material showed good specific capacitance and energy density but very low power density than other reports.[134]

Li *et al.* prepared 3D porous MnO_2@carbon nanosheets synthesized from rambutan peel. They fabricated an asymmetric SC of MnO_2@R//NR-800 by using the MnO_2@R composite material as a positive electrode and NR-800 as a negative electrode. The results showed a low specific capacitance of 139.6 F g^{-1} at very low current density. It showed cycling life *i.e.*, 92% capacitance retention after 5000 charge–discharge cycles with an energy density of 9.2 W h kg^{-1} and good power density of 1283.7 W kg^{-1}.[135]

Li *et al.* reported MnO_2 nanosheets derived from agaric grown on biomass-derived N-doped carbon for an asymmetric SC. The composite material showed good electrochemical performance due to the 3D pore structure and large specific surface area. It exhibited a specific capacitance of 330 F g^{-1} at 1 A g^{-1} and very low cyclic stability *i.e.*, 75% capacitance retention after 1000 cycles. Also, the electrode showed a low energy density of 28 W h kg^{-1} at a power density of 560 W kg^{-1}.[136]

Li *et al.* fabricated a MnO_x nanosheet anchored on lotus seed pod-derived carbon composite for a high-performance SC. The prepared MnO_x@LSCF hybrid electrode material comprised a 3D conductive network and ultrathin MnO_x nanosheets with oxygen vacancies, which can boost intrinsic electron and ion transmission and allow for adequate surface faradaic redox reactions. The electrode material showed a specific capacitance of 406 F g^{-1} with a capacitance retention

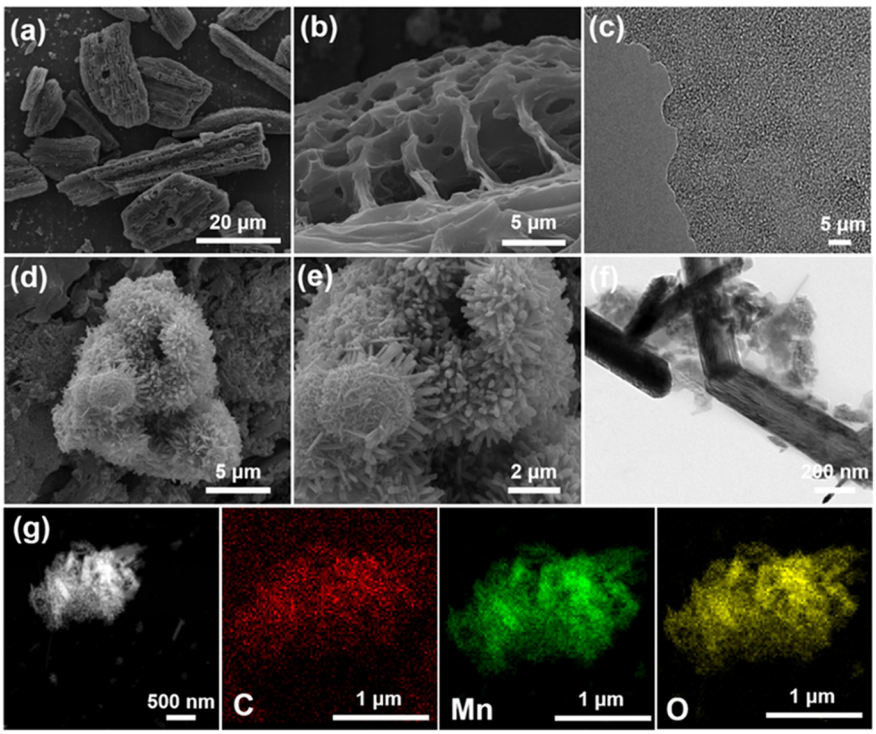

Fig. 11 (a and b) SEM images of BL-3, (c) TEM image of BL-3, (d and e) SEM images of MnO_2@BL-3 h, (f) TEM image of MnO_2@BL, and (g) MnO_2@BL-3-6 h EDS map. Reproduced from ref. 138 with permission from ACS, copyright 2023.

of 91% after 5000 cycles. The material delivered low energy as well as power density.[137]

Yu *et al.* fabricated an electrode material for an SC from a MnO_2 nanosheet composite with bamboo leaf (MnO_2@BL) carbon. The SEM and TEM images of BL and MnO_2@BL are depicted in Fig. 11 along with the EDS map. A specific capacitance of 76 F g^{-1} was achieved at a current density of 0.5 A g^{-1}. It showed a 14% loss for 5000 cycles.[138]

Nanowires

Yang *et al.* fabricated a porous 3D structure of MnO_2 nanowires and hemp stem-derived AC (HC) as an electrode material for SC application. It exhibited a specific capacitance of 340 F g^{-1} at 1 A g^{-1} current density with 12% capacitance loss after 3000 cycles. The electrochemical performance was measured in a three-electrode assembly using 1 m Na_2SO_4 as an electrolyte. For the asymmetrical SC, 3D HC as the anode and 3D MnO_2/HC as the cathode were used. The electrode material exhibited a specific energy of 33.3 W h kg^{-1} at a specific power density of 14.8 W kg^{-1}.[139]

The work done by Mohammed *et al.* demonstrated a hybrid SC device. The MnO_2 nanowires were decorated on the *Faidherbia Albida* fruit shell (FAFSC) carbon sphere. They fabricated a symmetric device using MnO_2/FAFSC as a negative and positive electrode while MnO_2/FAFSC as a negative electrode for an asymmetric SC. The composite electrode material showed electrochemical performance in two different electrolytes such as 3 M KOH and 1 M Na_2SO_4. It revealed specific capacitances of 426 F g^{-1} and 202.5 F g^{-1} in 3 M KOH and 1 M Na_2SO_4 respectively. The electrode material delivered a good cycle life of 97% capacitance retention after 1000 cycles. Also, it exhibited 32 W h kg^{-1} energy density at 400 W kg^{-1} power density.[140]

Zang *et al.* synthesized a MnO_2/biomass-derived carbon composite using silkworm excrement. The thin and flower-like MnO_2 nanowires were decorated on biomass-derived carbon. The hybrid electrode material displayed a specific capacitance of 238 F g^{-1} at 0.5 A g^{-1} current density of 1 M Na_2SO_4. It exhibited an energy density of 38.6 W h kg^{-1} at a power density of 698 W kg^{-1} with 7% capacitance loss for 2000 cycles.[141]

Nanorods

Shen *et al.* fabricated a δ-MnO_2/soybean stalk carbon composite electrode material which delivered a superior specific capacitance of 530 F g^{-1} at 0.2 A g^{-1}. It showed better cycling stability with 91% capacitance retention after 6000 consecutive charge–discharge cycles with an energy density of 5607 W h kg^{-1} at a power density of 90 W kg^{-1}.[142]

For a high-energy asymmetric SC, Nirmaladevi *et al.* synthesized MnO_2 nanorods with carbon derived from *Acacia leucophloea* wood sawdust. Electrochemical characteristics were determined using three and two electrode set ups. The composite material revealed a specific capacitance of 290 F g^{-1} in the two-electrode cell configuration and 512 F g^{-1} in the three-electrode assembly at a current density of 0.5 A g^{-1} and 7% capacitance loss for 10 000 cycles. The electrode materials showed an energy density and power density of 74.3 W h kg^{-1} and 1996.4 W kg^{-1} respectively.[143]

Nanoflakes

Yuan *et al.* successfully synthesized a hierarchically porous MnO_2 nanoflakes/rice husk-derived carbon composite as an electrode material for an SC. The MnO_2 film was composed of well-dispersed nanoflakes that anchored on the surface of rice husks for adequate structural stability. The composite material showed electrochemical properties in 0.5 M Na_2SO_4 electrolyte. The material exhibited a specific capacitance of 197.6 F g^{-1} at 5 mV s^{-1} scan rate and 210.3 F g^{-1} at 0.5 A g^{-1}. The composite displayed a 20% capacitance loss for 5000 charge–discharge cycles.[144]

Hu *et al.* synthesized MnO_2/poly(3,4-ethylene dioxythiophene) core–shell nanoflakes on ramie-derived fiber. The electrochemical performances shown in Fig. 12 were measured using a two-electrode assembly in PVA/KCl gel solid-state electrolyte. The hybrid electrode material revealed a high specific capacitance of 922 F g^{-1} at 1 A g^{-1}. The fabricated flexible solid-state symmetric device showed a specific capacitance of 138 F g^{-1} at a current density of 1 A g^{-1} and 17% capacitance loss after 10 000 cycles. It showed an energy density of 19.17 W h kg^{-1} at a power density of 500 W kg^{-1}.[145]

Nanoneedles

Biowaste-derived carbon from human hair (Acs) was synthesized by Deng *et al.*, and decorated with a needle-like morphology of MnO_2. The ACs and MnO_2 were synthesized in different weight ratios *i.e.*, ACs/$KMnO_4$ = 1 : 2, 1 : 1, 2 : 1, 4 : 1, 8 : 1, 10 : 1, 12 : 1, 14 : 1 and 16 : 1. Then, MnO_2/ACs (1 : 12) delivered a specific capacitance of 300 F g^{-1} after 500 cycles in 1.0 M H_2SO_4. The MnO_2/ACS (1 : 12) electrode material showed capacitance values of 410 F g^{-1}, 345 F g^{-1}, and 251 F g^{-1} in 1 M H_2SO_4, 1 M KOH, and 1 M Na_2SO_4 aqueous electrolyte respectively. Therefore, the electrode material exhibited the highest capacitance value in 1 M H_2SO_4 electrolyte solution.[146]

Nano wrinkles

Yuan *et al.* fabricated a prototype asymmetric SC device using chicken bones as a 3D hierarchical porous carbon scaffold (HPCS) and MnO_2 composite. They reported that MnO_2 showed a nano wrinkle morphology when it was deposited on the 3D-HPCS template. Electrochemical performance was measured using two and three-electrode cell configurations in 1 M Na_2SO_4 aqueous electrolytic solution. The composite electrode material revealed a specific capacitance of 476.4 F g^{-1} at a current density of 1 A g^{-1} and approximately 84.9% capacitance retention for 4000 cycles. The electrode material exhibited a specific energy of 60.8 W h kg^{-1} at a power density of 20.7 W kg^{-1}.[147]

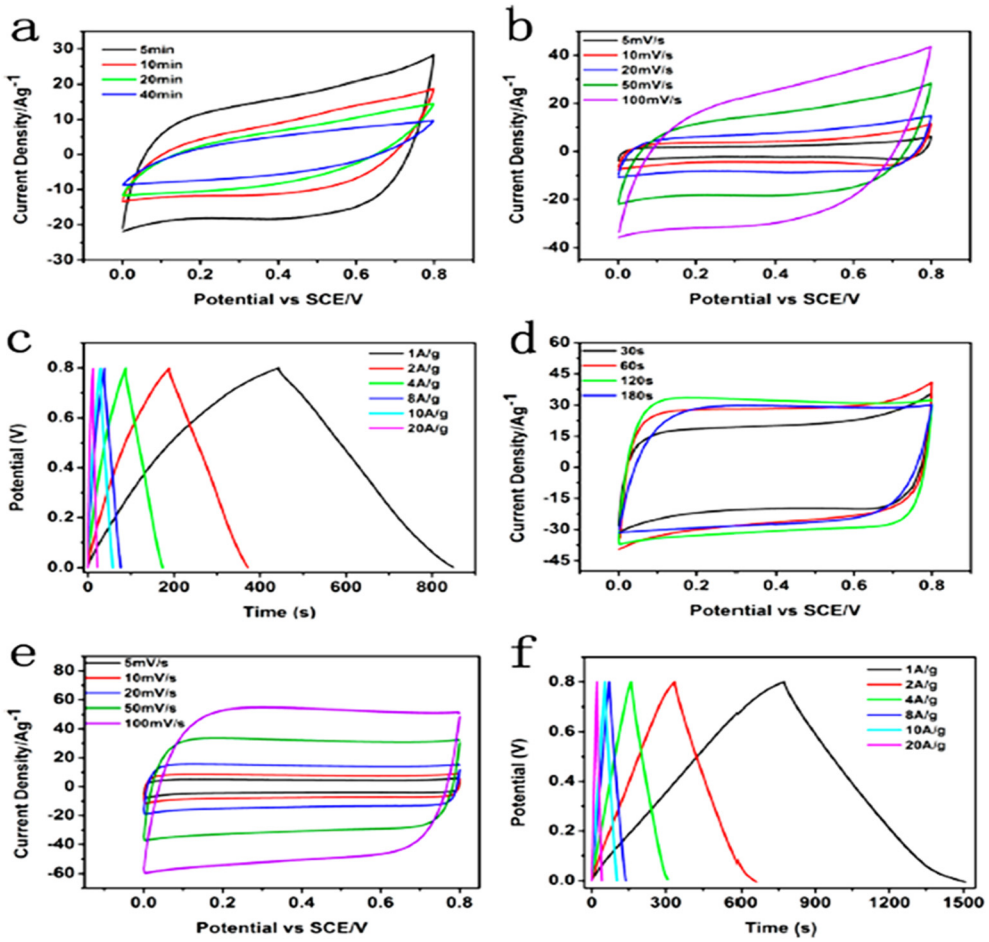

Fig. 12 (a) CV curves of the RCFs/MnO_2 electrodes with different electrodeposition times at 50 mV s^{-1}. (b) CV curves at varied potential scan rates of the RCFs/MnO_2 electrode with MnO_2 deposited for 5 min. (c) Charge–discharge curves at different current densities of the RCFs/MnO_2 electrode with MnO_2 deposited for 5 min. (d) CV curves of the RCFs/MnO_2/PEDOT electrodes with different polymerization times at 50 mV s^{-1}. (e) CV curves at varied potential scan rates of the RCFs/MnO_2/PEDOT electrode with PEDOT deposited for 120 s. (f) Charge–discharge curves at different current densities of the RCFs/MnO_2/PEDOT electrode with PEDOT deposited for 120 s. Reproduced from ref. 145 with permission from ACS, copyright 2016.

Nanoplates

For a high-performance asymmetric SC, Li *et al.* fabricated MnO_2 nanoplates on biomass-derived carbon nanosheets from Willow Catkin. Interconnected thin carbon nanosheets behave as 3D conductive networks which is useful for rapid electron transmission. The electrode material tests were carried out using three electrode assemblies in 1 M Na_2SO_4. The composite electrode material exhibited a gravimetric capacitance of 188 F g^{-1} at 5 mV s^{-1}. It showed superior cycling performance with only 1.4% capacitance loss after 10 000 charge–discharge cycles with 23.6 W h kg^{-1} energy density at 188.8 W kg^{-1} power density.[148]

Nanowalls

In the work done by Wang *et al.*, they synthesized δ-MnO_2/carbon sheets from biomass-derived cornstalk for an SC. Due to the synergic effects of δ-MnO_2 nanowalls and biomass-derived carbon nanosheets, the hybrid electrode material showed a significant specific capacitance of 520 F g^{-1} at 1 mV s^{-1} scan rate in Na_2SO_4, but it suffered from poor cyclic stability. A 20% capacitance loss was observed after 5000 charge–discharge cycles.[149]

Others

Lu *et al.* synthesized a biomass-derived carbon from activated *Ganoderma lucidum* spore and pompon-like MnO_2 composite. In this case, the morphology of MnO_2 was rare and unique. O and N heteroatoms were used to enhance the electrochemical properties such as surface polarity, reaction activity, wettability, and electronic conductivity. The electrochemical performances are depicted in Fig. 13. The composite material delivered a remarkable specific capacitance of 1324 F g^{-1} at 1 A g^{-1} current density using an electrode system in a 6 M KOH aqueous electrolyte. Although the electrode material showed a significant energy density of 43.75 W h kg^{-1} it suffers from low power density *i.e.*, 250 W

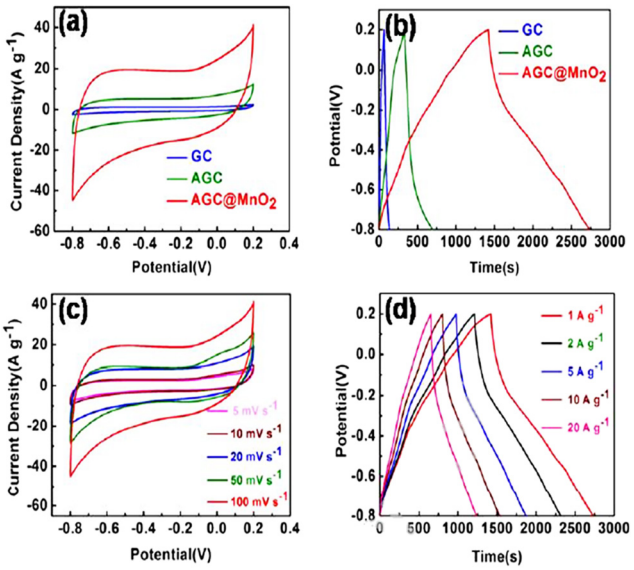

Fig. 13 (a) CV curves of GC, AGC, and AGC@MnO_2 at 100 mV s^{-1}. (b) GCD curves of GC, AGC, and AGC@MnO_2 at 1 A g^{-1}. (c) CV curves of AGC@MnO_2 at different scan rates. (d) GCD curves of AGC@MnO_2 at 1, 2, 5, 10, and 20 A g^{-1}. Reproduced from ref. 150 with permission from Elsevier, copyright 2020.

kg^{-1}. It showed 92.3% capacitance retention after 5000 charge–discharge cycles.[150]

Tan *et al.* synthesized the composite of MnO_2 with sisal hemp active carbon (SHAC) and used it as an electrode material which showed a specific capacitance of 397.9 F g^{-1}. An asymmetric SC was assembled by employing flower-like MnO_2/SHAC as the positive electrode and layered SHAC as the negative electrode. It exhibited capacitance retention of 80.4% after 5000 cycles. The electrode material revealed an energy density and superior power density of 46.2 W h kg^{-1} and 3679.5 W kg^{-1} respectively.[151]

Li *et al.* prepared an asymmetric all solid-state SC from biomass waste-derived carbon from corncob and MnO_2 composite. The MnO_2@corncob composite material delivered an excellent electrochemical performance in PVA/LiCl gel electrolyte. The composite electrode material revealed an areal specific capacitance of 3455 mF cm^{-2} at 1 mA cm^{-2} and only 1% loss of capacitance was observed after 10 000 cycles. It exhibited a very low energy and power density of 1.56 mW h cm^{-2} and 900 mW cm^{-2} respectively.[152]

Yu *et al.* synthesized *Typha orientalis* leaves biomass-derived P-doped porous carbon and MnO_2 hybrid electrodes for high-performance SCs. The electrode material delivered a specific capacitance of 384 F g^{-1} in 1 M KOH at 1 A g^{-1} current density. The fabricated asymmetric SC device displayed an energy density of 46 W h kg^{-1} at a high-power density of 1000 W kg^{-1}. However, it showed a huge capacitance loss *i.e.* 17% after 10 000 cycles.[153]

Konnerth *et al.* synthesized MO-doped AC from biomass-derived materials such as bakery waste and coffee grounds. They used MOs such as Fe_2O_3, Fe_3O_4, and MnO_2, to fabricate composites with bakery waste and coffee grounds. The electrochemical performance tests were carried out in 0.5 M H_2SO_4 aqueous electrolyte. The better electrochemical results were obtained for the AC spent coffee ground-MnO_2 electrode material. An 875 F g^{-1} specific capacitance achieved at 5 mV s^{-1} scan rate and 40.3 F g^{-1} was observed for bakery waste containing Fe_2O_3 doping.[154]

The work done by Palem *et al.* synthesized carboxymethyl cellulose with a CuO@MnO_2 hybrid material. The material showed good electrochemical performance due to its unique nanocrystalline morphology. The electrochemical properties were measured in 3 M KOH as an electrolyte. This composite material showed a specific capacitance of 414 F g^{-1} at 0.5 A g^{-1} current density with 96.2% capacitance retention after 5000 cycles.[155]

The experiment performed by Wen *et al.* used disposable bamboo chopsticks and converted them into carbon fibers. MnO_2 was grown on carbon fiber to obtain a composite material. The MnO_2 nanoparticles were observed on the surface of carbon fibers which are clearly shown in Fig. 14. The self-supported and binder-free composite electrode material showed better electrochemical performance in aqueous 1 M Na_2SO_4 solution. The composite material exhibited a specific capacitance of 375 F g^{-1} at 1 A g^{-1} and outstanding capacitance retention *i.e.*, 110.3% was achieved after 5000 cycles. The symmetric SC consists of carbon fiber and MnO_2 electrodes delivering an energy density of 11 W h kg^{-1} at 17.4 kW kg^{-1} power density.[156]

A three-dimensional hybrid kenaf stem-derived porous carbon and MnO_2 composite was prepared by Wang *et al.*, for a high-performance SC. The three-dimensional porous structure of carbon (as shown in Fig. 15) delivered a conductive network to enhance the charge transport and mass transfer in the electrochemical process and improve

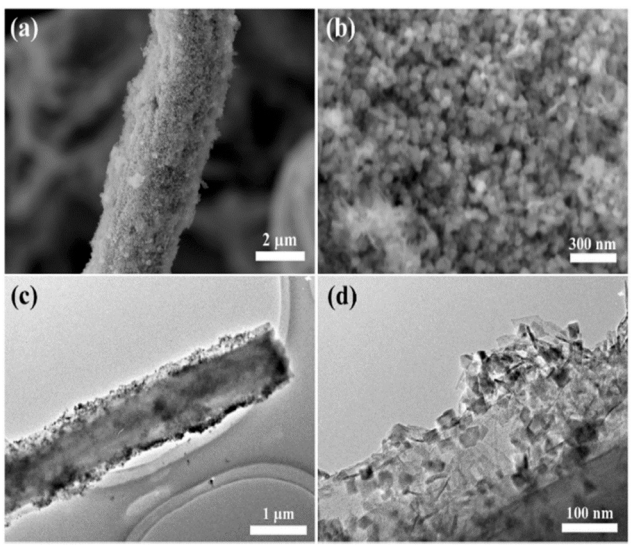

Fig. 14 (a) SEM images and (b) corresponding enlarged view of CFS/MnO_2. (c) TEM image and (d) corresponding enlarged view of CFS/MnO_2. Reproduced from ref. 156 with permission from Elsevier, copyright 2017.

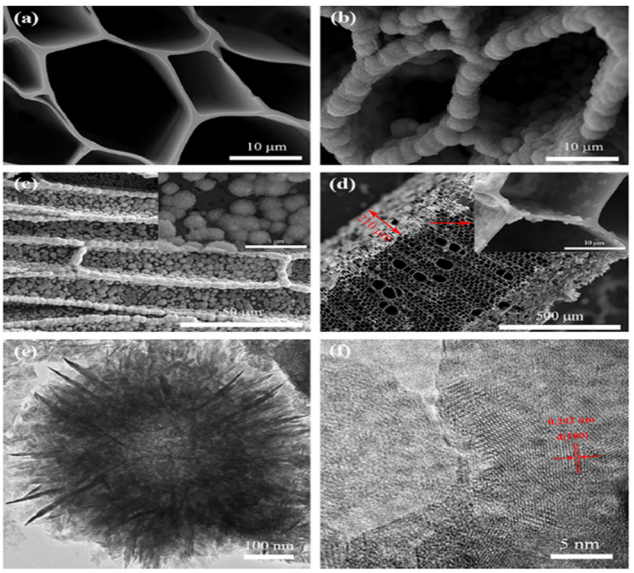

Fig. 15 (a) SEM image of 3D-PC. (b–d) SEM images of MnO_2/3D-PC after a 200 min deposition. (b) Top view. (c) Side view. (d) Cross-section. TEM (e) and HRTEM (f) images of MnO_2/3D-PC. Reproduced from ref. 157 with permission from Elsevier, copyright 2014.

large MnO_2 mass loading capacity. The specific capacitance achieved by the composite material was 416 F g^{-1} at a scan rate of 1 mV s^{-1} with the lowest energy density as well as power density of 17.3 W h kg^{-1} and 198 W kg^{-1} respectively. Moreover, it also suffers from low cyclic stability *i.e.*, 86% capacitance retention after 1000 cycles.[157]

Yang and Park synthesized MnO_2/biomass-derived 3D porous carbon from banana peel by a hydrothermal method. The pore images of the BPC composite are shown in Fig. 16.

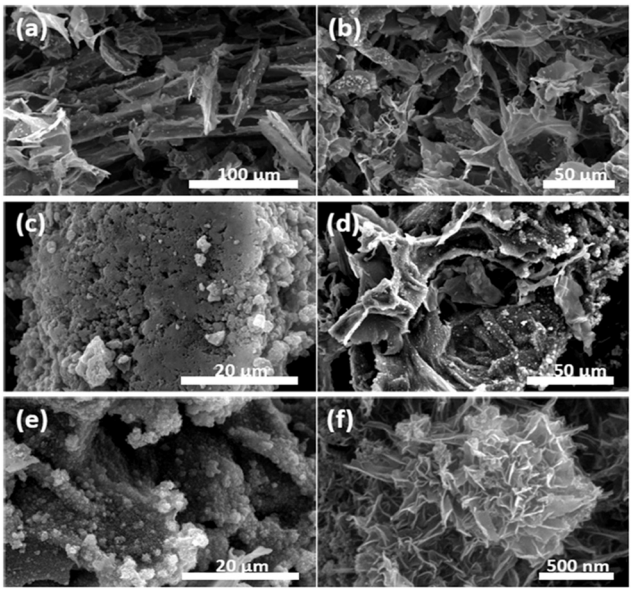

Fig. 16 SEM images of (a and b) BPC at different magnifications, (c) MnO_2 particles, and (d–f) MnO_2/BPC composites at different magnifications. Reproduced from ref. 158 with permission from Elsevier, copyright 2018.

Due to the 3D porous structure, the material showed good electrochemical performance. The electrochemical tests were carried out using three-electrode cell configurations in 1 M Na_2SO_4 aqueous electrolyte. The composite material exhibited a gravimetric capacitance of 139.6 F g^{-1} at 300 mA g^{-1}. Also, it delivered a good cyclic life of 92.3% capacitance retention after 1000 cycles.[158]

Wang *et al.* fabricated a device using MnO_2/orange peel as the biomass-derived material for a solid-state carbon-based SC. The schematic illustration of the synthesized material and characterization techniques such as XRD, XPS, SEM, TEM, and HRTEM are shown in Fig. 17. The electrochemical performance of the electrode material was measured using a three-electrode assembly in 1 M Na_2SO_4 while PVA gel electrolyte was used for the device. The composite material displayed 186 F g^{-1} gravimetric capacitance and areal capacitance of 3987 mF cm^{-1}. The material showed huge capacitance loss *i.e.* 16%.[159]

For a high-performance SC, Liu *et al.* deposited MnO_2 nanostructures on graphene-like porous carbon nanosheets (GPCN-SS). The SEM and TEM images of porous carbon and MnO_2/GPCN-SS composites are shown in Fig. 18. Due to the synergistic effect of GPCN-SS and MnO_2 nanostructures, the composite material showed a gravimetric specific capacitance of 438 F g^{-1} at a current density of 0.5 A g^{-1}. The asymmetric SC was prepared with the MnO_2/GPCN-SS composite as the cathode and GPCN-SS as the anode. Moreover, the MnO_2/GPCN-SS electrode material displayed an energy density of 50.2 W h kg^{-1} at 516 W kg^{-1} power density. However, 22% of capacitance loss was observed for 10 000 cycles.[160]

Ping *et al.*, in their work, incorporated MnO_2 with biomass-derived porous carbon from natural *Juncus effusus*. The electrochemical performances were measured in a neutral 1 M Na_2SO_4 electrolyte. The composite material delivered a low specific capacitance of 238 F g^{-1} at 1 A g^{-1}. The energy density and power density for the symmetric device were 19.13 W h kg^{-1} and 225 W kg^{-1}. However, it suffered from poor cyclic stability and very huge capacitance loss *i.e.* 14% after 5000 cycles.[161] Yumak *et al.* successfully synthesized biomass-derived AC from Kanlow switchgrass and decorated it with MnO_2. The specific surface area of the material increased by direct KOH and H_3PO_4 activation. Fig. 19 shows the SEM images of materials. However, a notable effect was observed for the KOH-activated biochar. The hybrid composite material showed low specific capacitance of 110 F g^{-1} for 1000 cycles in a 6 M KOH aqueous electrolyte.[162]

For a high-performance SC, Du *et al.* synthesized an electrode material from a wheat flour-derived matrix decorated with MnO_2 nanoparticles. The synthesized materials were characterized by SEM, TEM, HRTEM, and elemental mapping along with the SAED pattern as shown in Fig. 20. The electrode material exhibited a specific capacitance of 197 F g^{-1} at 1 A g^{-1} current density with a remarkable capacitance retention of 100% after 5000 cycles. The symmetric SC was prepared with WFC@MnO_2 as positive

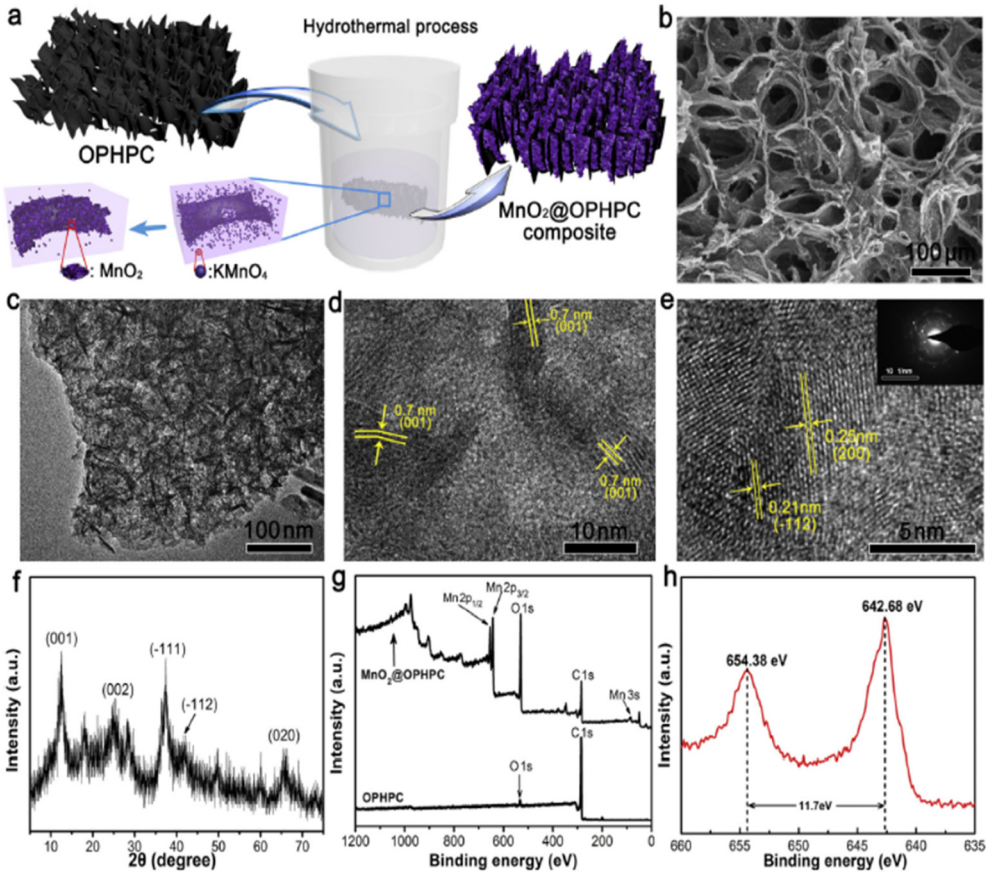

Fig. 17 (a) The schematic illustration of the fabrication of the MnO_2@OPHPC composite. (b) SEM image, (c) TEM image, and (d and e) HRTEM images of MnO_2@OPHPC. (f) XRD of MnO_2@OPHPC, (g) survey XPS spectra of OPHPC and MnO_2@OPHPC, and (h) Mn 2p core-level XPS spectrum of MnO_2@OPHPC. Reproduced from ref. 159 with permission from Elsevier, copyright 2018.

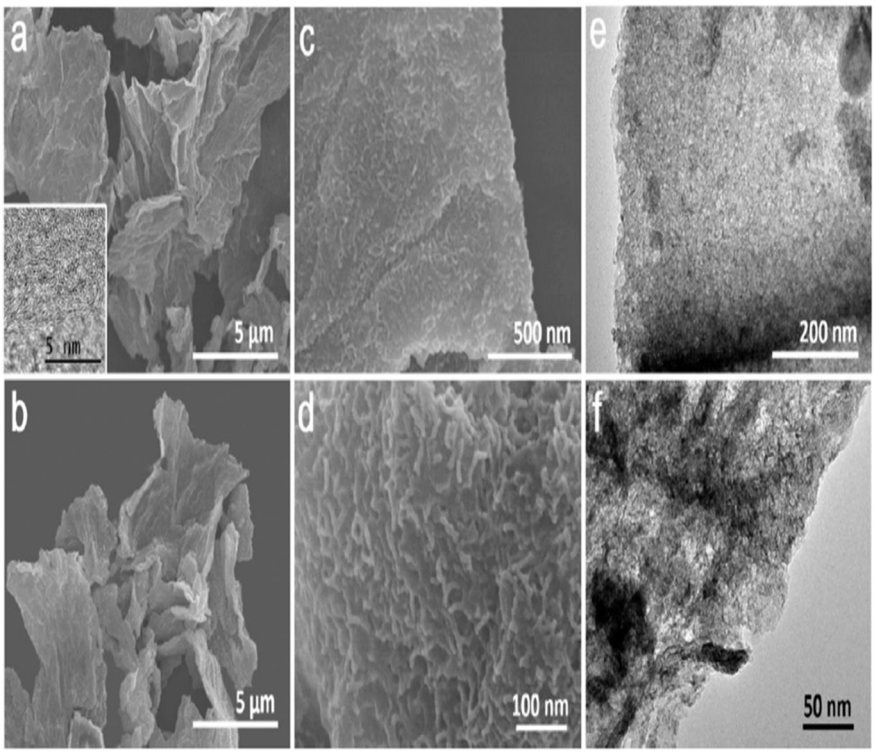

Fig. 18 SEM images of GPCN-SS (a) and MnO_2/GPCN-SS (b–d) at different magnifications; the inset of (a) shows the HRTEM image of GPCN-SS. (e and f) TEM images of MnO_2/GPCN-SS at different magnifications. Reproduced from ref. 160 with permission from ACS, copyright 2019.

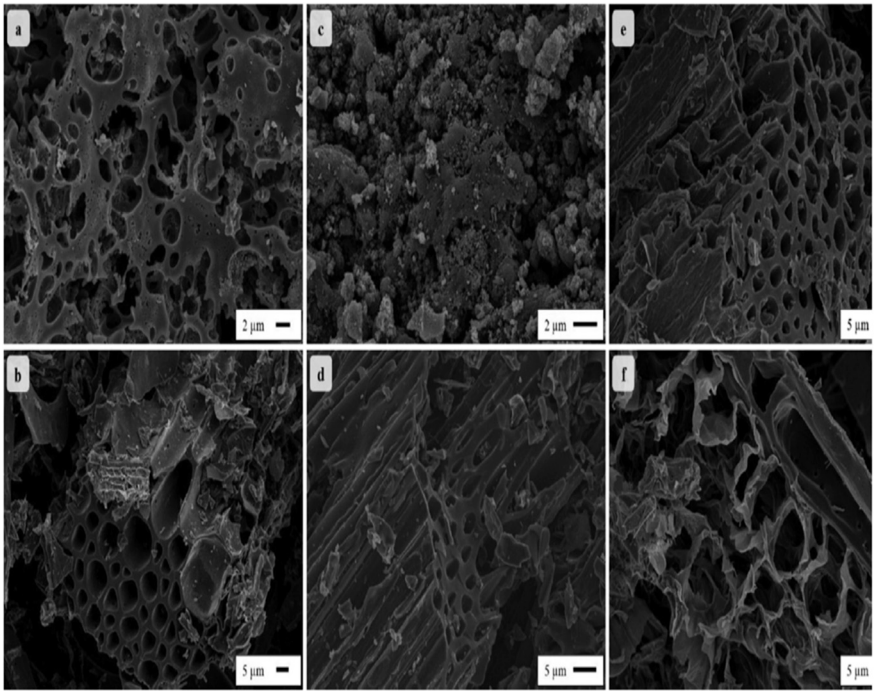

Fig. 19 SEM microstructures of the activated carbons: a) KOH-K, b) KOH-KB, c) H_3PO_4-K, d) H_3PO_4-KB, e) MnO_2/KOH-KB, and f) MnO_2/H_3PO_4-KB. Reproduced from ref. 162 with permission from Elsevier, copyright 2020.

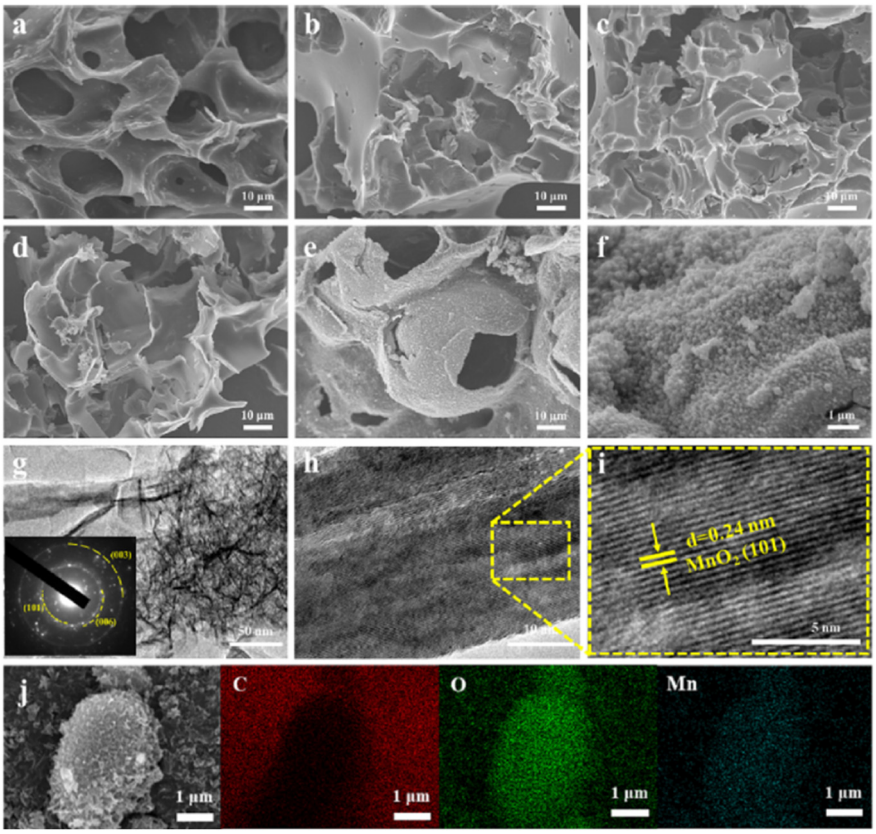

Fig. 20 SEM images of (a) WFC-0, (b) WFC-2, (c) WFC-4, (d) WFC-6, (e and f) WFC-4@MnO_2, (g and h) TEM images of WFC-4@MnO_2, the inset shows the corresponding SAED pattern from the edge of MnO_2, and (i) HRTEM image of WFC-4@MnO_2. (j) Element mapping images of C, O, and Mn. Reproduced from ref. 163 with permission from Elsevier, copyright 2023.

Table 2 Latest reports on MnO_2 and biomass-derived carbon composites for SCs

Sr. no.	Morphology of metal oxide	Biomass-derived carbon	Specific capacitance ($F g^{-1}$)	Scan rate/current density	Energy density ($W h kg^{-1}$)	Power density ($W kg^{-1}$)	Cyclic stability (capacitance retention %, cycles)	Electrolyte	Ref.
1.	MnO_2 nanorods	Sweet potato	718	10 mV s^{-1}	66.4	1980	89%, 5000	1 M Na_2SO_4	164
2.	Two-dimensional layered δ-MnO_2	Bamboo fibre	364.4 (2E)	0.5 A g^{-1}	12.6	164	99.7%, 10 000	6 M KOH	165
3.	MnO_2/CuO/rGO	Lemon peel	177	2 A g^{-1}	79.60	2430	90%, 10 000	1 M Na_2SO_4	166
4.	MnO_2	Eggplant	652	0.5 A g^{-1}	—	—	79.2%, 10 000	1 M Na_2SO_4	167
5.	MnO_2	Wood	87	1 A g^{-1}	12.2	22.3	75.2%, 10 000	—	168
6.	MnO_2	*Datura stramonium* seedpod	700	5 mV s^{-1}	—	—	86%, 3000	0.5 M Na_2SO_4	169
7.	MnO_2 nanofibers	Pineapple leaf	195	0.1 A g^{-1}	26.8	120.5	84.5%, 10 000	1 M H_2SO_4	170
8.	δ-MnO_2 nanosheets	Lignin	198	—	3.82	125	—	—	171
9.	MnO_2 nanoflowers	Bacterial cellulose	170	1 A g^{-1}	9.8	10 500	76%, 5000	1 M Na_2SO_4	172
10.	MnO_2	Luffa sponge	586	1 A g^{-1}	31.4	400	95%, 20 000	0.5 M Na_2SO_4	173
11.	δ-MnO_2	Reed residue	128.75	0.5 A g^{-1}	22.7	15.1k	98.7%, 10 000	1 M Na_2SO_4	174
12.	MnO_2	Wood tracheids	13.55 F cm^{-2}	10 mA cm^{-2}	0.875 mW cm^{-2}	9 mW cm^{-2}	93.21%, 10 000	1 M Na_2SO_4	175

and negative electrodes which resulted in an energy density of 17.1 W h kg^{-1} at an excellent power density of 11 000 W kg^{-1} and only 5% loss of capacitance retention after 5000 charge–discharge cycles.[163]

Table 2 highlights the latest reports on MnO_2 and biomass-derived carbon composites for SC applications. Notably, these studies emphasize on the morphology of MnO_2 and electrochemical studies of composite materials.

Recent reports on MnO_2 and several carbon-based composite electrode materials for SCs obtained from different biomasses are shown in Table 2. It illustrates the specific capacitance, power density, current density, scan rate, cyclic stability, and various electrolytes used in electrochemical reactions. Different shapes of MnO_2 such as nanorods, nanofibers, nanosheets, and nanoflowers were mentioned. Most of the experiments were conducted using plant-derived carbon. In the studies, the electrolytes Na_2SO_4, KOH, and H_2SO_4 were widely used. The table elucidates that the highest specific capacitance reported in MnO_2 nanorod and carbon derived from sweet potato material is 718 F g^{-1} with 10 mV s^{-1} scan rate. Although it has a low energy density and power density, the two-dimensional layered δ-MnO_2 and biomass-generated carbon from bamboo fiber exhibits exceptional cyclic stability, with 99.7% after 10 000 cycles. The outstanding power density of 15.1 kW kg^{-1} with good capacitance retention of 98.7% after 10 000 cycles is revealed by δ-MnO_2 and carbon generated from reed residue waste. MnO_2 and carbon made from bacterial cellulose have good power densities of 10 500 W kg^{-1} but have low specific energies and energy densities of 170 F g^{-1} and 9.8 W h kg^{-1}, respectively. With a specific capacitance of 177 F g^{-1} at 2 A g^{-1} current density and an energy density of 79.60 W h kg^{-1} at a power density of 2430 W kg^{-1}, the MnO_2/CuO/r-GO composite with carbon generated from lemon peel was employed to synthesize an electrode material. The lowest specific capacitance, energy density, and power density were found in the MnO_2 and carbon produced from wood tracheids, with values of 13.55 F cm^{-2}, 0.875 mW h cm^{-2}, and 9 mW cm^{-2}, respectively. MnO_2 and carbon produced from wood have poor cycle stability. In most of the reports, electrochemical testing was done using a three-electrode assembly.

5. Conclusions and future perspective

This review offered information about recent advancements in MnO_2 and biomass-derived carbon-based composites for SC application. The electrochemical properties of SCs are affected by electrode materials, preparation process, and electrolytes. Thus, the selection of electrode material plays an important role in achieving good electrochemical properties. As the analyzed literature reports suggest, MnO_2 is a famous supercapacitive electrode material among all TMOs due to its various advantages. The types and morphologies of MnO_2 play an important role in the final electrochemical performance of the material. However, MnO_2 suffers from low electrical conductivity and poor stability and it was found that this weakness can be overcome by preparing composites of MnO_2 with different materials. Like MnO_2, biomass-derived carbon materials have also received increased attention in the field of energy storage devices. Here, we collectively reported various biomass precursors to obtain the carbon materials and the properties of carbon such as structural features, surface area, and porosity. It was observed

that biomass-derived carbon is synthesized from a variety of materials such as crops, plants, animals, and waste biomass. Due to high porosity, the carbon provides several active sites for the electrolyte ions resulting in enhanced stability and specific capacitance. The carbon can be combined with MnO_2 to achieve better electrochemical performances. In fact, all the examples of MnO_2-biomass-derived carbon-based materials discussed above proved this point. The future research in this area will be continued along following main directions.

The first main approach involves development of newer and more efficient synthesis techniques both for MnO_2 and carbon. Although most of the synthesis methods are well-optimized to obtain MnO_2 with desired features there is still considerable scope for the development of *in situ* methods that will directly form the film of material on the desired substrate to be used as an electrode. The new developments in thin film technologies have come up with several efficient methods but they need to be adapted or suitably modified to obtain complex shapes (such as core–shell or porous) of the desired materials. Layer by layer assembly of the materials is also a requirement in some applications. Meanwhile, almost all reports about biomass-derived carbon have used pyrolysis and carbonization methods at high temperatures in an inert atmosphere to obtain the carbon. As these methods require high energy, a one-step preparation process that yields the highest quality carbon at the lowest possible temperatures should be invented under the advocacy of energy saving and emission reduction. So far, in the real application of SCs, the flexibility of electrodes and cyclic stability of the electrode materials are highly valued. So, there is a need to develop efficient synthesis methods that will yield stable electroactive materials sustainable under various conditions.

As far as electrochemical testing is concerned, the most used electrolytes are still Na_2SO_4, KOH, H_2SO_4, *etc.* So, there is a need to develop and test new electrolytes that are more stable as well as less corroding in nature and can offer wide potential windows. Polymer or gel-based electrolytes that can be used in all solid-state devices need to be tested and compared. The use of non-aqueous or solid electrolytes sounds more practical towards device fabrication but it will need detailed studies about the electrode–electrolyte (solid–solid or solid–gel) interfaces that will reveal the mechanisms of energy storage and conduction. The interface barriers (resistance) should be minimized by using suitable surface modification techniques for the electrodes or by inventing electrolytes compatible with different electrode materials. For this purpose, functional polymer-based electrolytes are being investigated with great interest.

Another important consideration is the film forming property and processability of various materials developed. The thin films of MnO_2 and carbon-based active electrodes influence the faradaic processes at the electrode–electrolyte interface. Not all materials or composites give stable films. Hence there is a need to develop composite materials that are adherent with excellent film-forming properties on various substrates such as nickel foam, graphite, carbon cloth *etc.* to give the best electrochemical performance. To summarise, significant efforts should be made to develop new and efficient composite electrode materials to be included in flexible and compressible SC devices.

Conflicts of interest

There are no conflicts of interest to declare.

References

1 P. H. Patil, V. V. Kulkarni and S. A. Jadhav, *J. Compos. Sci.*, 2022, **6**, 363.
2 P. H. Patil, V. V. Kulkarni, A. K. Mane, T. D. Dongale and S. A. Jadhav, *Polym. Adv. Technol.*, 2024, **35**, e6362.
3 V. S. Patil, S. S. Thoravat, S. S. Kundale, T. D. Dongale, P. S. Patil and S. A. Jadhav, *Chem. Phys. Lett.*, 2023, **814**, 140334.
4 G. Smdani, M. R. Islam, A. N. Ahmad Yahaya and S. I. Bin Safie, *Energy Environ.*, 2023, **34**, 1094–1141.
5 L. Lai, H. Yang, L. Wang, B. K. Teh, J. Zhong, H. Chou, L. Chen, W. Chen, Z. Shen, R. S. Ruoff and J. Lin, *ACS Nano*, 2012, **6**, 5941–5951.
6 L. Xie, G. Sun, F. Su, X. Guo, Q. Kong, X. Li, X. Huang, L. Wan, W. Song, K. Li, C. Lv and C.-M. Chen, *J. Mater. Chem. A*, 2016, **4**, 1637–1646.
7 E. Frackowiak and F. Béguin, *Carbon*, 2001, **39**, 937–950.
8 V. V. Kulkarni, P. H. Patil, T. D. Dongale, A. V. Takaloo and S. A. Jadhav, *Chem. Phys. Lett.*, 2024, **841**, 141173.
9 B. K. Kim, S. Sy, A. Yu and J. Zhang, in *Handbook of Clean Energy Systems*, ed. J. Yan, Wiley, 1st edn, 2015, pp. 1–25.
10 M. Sevilla and R. Mokaya, *Energy Environ. Sci.*, 2014, **7**, 1250–1280.
11 P. Forouzandeh, V. Kumaravel and S. C. Pillai, *Catalysts*, 2020, **10**, 969.
12 S. Rajagopal, R. Pulapparambil Vallikkattil, M. Mohamed Ibrahim and D. G. Velev, *Condens. Matter*, 2022, **7**, 6.
13 A. Diallo, N. Tandjigora, S. Ndiaye, T. Jan, I. Ahmad and M. Maaza, *SN Appl. Sci.*, 2021, **3**, 562.
14 S. A. Jadhav, V. V. Kulkarni, P. H. Patil and I. U. Shah, *J. Appl. Electrochem.*, 2023, **53**, 1911–1926.
15 M. Vangari, T. Pryor and L. Jiang, *J. Energy Eng.*, 2013, **139**, 72–79.
16 J. Hong, H. Kim, J. E. Lee, Y. N. Ko, K. T. Park, Y. E. Kim, M. H. Youn, S. K. Jeong, J. Park and W. Lee, *Korean J. Chem. Eng.*, 2020, **37**, 1218–1225.
17 V. V. Kulkarni, P. H. Patil and S. A. Jadhav, *Period. Polytech., Chem. Eng.*, 2024, **68**, 1–15.
18 B. T. Sone, X. G. Fuku and M. Maaza, *Int. J. Electrochem. Sci.*, 2016, **11**, 8204–8220.
19 B. T. Vetrikarasan, A. R. Nair, T. Karthick, S. K. Shinde, D. Y. Kim, S. N. Sawant and A. D. Jagdale, *J. Energy Storage*, 2023, **72**, 108403.
20 J. Wei, F. Hu, X. Shen, B. Chen, L. Chen, Z. Wang, C. Lv and Q. Ouyang, *J. Colloid Interface Sci.*, 2023, **649**, 665–674.

21 A. C. Nwanya, M. M. Ndipingwi, C. O. Ikpo, R. M. Obodo, S. C. Nwanya, S. Botha, F. I. Ezema, E. I. Iwuoha and M. Maaza, *J. Alloys Compd.*, 2020, **822**, 153581.
22 J. B. K. Kana, J. M. Ndjaka, P. O. Ateba, B. D. Ngom, N. Manyala, O. Nemraoui, A. C. Beye and M. Maaza, *Appl. Surf. Sci.*, 2008, **254**, 3959–3963.
23 B. Padmadevi and T. Kalaivani, *Ceram. Int.*, 2022, **48**, 36101–36109.
24 J. Sackey, A. C. Nwanya, A. K. H. Bashir, N. Matinise, J. B. Ngilirabanga, A. E. Ameh, E. Coetsee and M. Maaza, *Mater. Chem. Phys.*, 2020, **244**, 122714.
25 A. Diallo, K. Kaviyarasu, S. Ndiaye, B. M. Mothudi, A. Ishaq, V. Rajendran and M. Maaza, *Green Chem. Lett. Rev.*, 2018, **11**, 166–175.
26 S. A. Jadhav, S. D. Dhas, K. T. Patil, A. V. Moholkar and P. S. Patil, *Chem. Phys. Lett.*, 2021, **778**, 138764.
27 T. S. Bhat, S. A. Jadhav, S. A. Beknalkar, S. S. Patil and P. S. Patil, *Inorg. Chem. Commun.*, 2022, **141**, 109493.
28 D. Wu, X. Xie, Y. Zhang, D. Zhang, W. Du, X. Zhang and B. Wang, *Front. Mater.*, 2020, **7**, 2.
29 R. Liang, Y. Du, P. Xiao, J. Cheng, S. Yuan, Y. Chen, J. Yuan and J. Chen, *Nanomaterials*, 2021, **11**, 1248.
30 A. Abdollahi, A. Abnavi, F. Ghasemi, S. Ghasemi, Z. Sanaee and S. Mohajerzadeh, *Electrochim. Acta*, 2021, **390**, 138826.
31 S. Azmi, A. Klimek and E. Frackowiak, *Mater. Today*, 2023, S1369702123002092.
32 J. Liu, J. Bao, X. Zhang, Y. Gao, Y. Zhang, L. Liu and Z. Cao, *RSC Adv.*, 2022, **12**, 35556–35578.
33 Y.-F. Li, S.-C. Zhu and Z.-P. Liu, *J. Am. Chem. Soc.*, 2016, **138**, 5371–5379.
34 R. Devi, V. Kumar, S. Kumar, M. Bulla, S. Sharma and A. Sharma, *Appl. Sci.*, 2023, **13**, 7907.
35 S. Sivakumar and L. Nelson Prabu, *Mater. Today: Proc.*, 2021, **47**, 52–55.
36 J. Liu, J. Bao, X. Zhang, Y. Gao, Y. Zhang, L. Liu and Z. Cao, *RSC Adv.*, 2022, **12**, 35556–35578.
37 P. Tagsin, P. Suksangrat, P. Klangtakai, P. Srepusharawoot, C. Ruttanapun, P. Kumnorkaew, S. Pimanpang and V. Amornkitbamrung, *Appl. Surf. Sci.*, 2021, **570**, 151056.
38 D. Kiymaz, A. Kiymaz, S. Tekoglu, F. Mayr, H. Dincalp and C. Zafer, *Thin Solid Films*, 2022, **762**, 139535.
39 M. He, L. Cao, W. Li, X. Chang and Z. Ren, *J. Alloys Compd.*, 2021, **865**, 158934.
40 R. A. Davoglio, G. Cabello, J. F. Marco and S. R. Biaggio, *Electrochim. Acta*, 2018, **261**, 428–435.
41 Y. Li, H. Xie, J. Wang and L. Chen, *Mater. Lett.*, 2011, **65**, 403–405.
42 S. Rong, P. Zhang, F. Liu and Y. Yang, *ACS Catal.*, 2018, **8**, 3435–3446.
43 B. Chettiannan, A. K. Srinivasan, G. Arumugam, S. Shajahan, M. AbuHaija and R. Rajendran, *ACS Omega*, 2023, **8**, 6982–6993.
44 P. H. Patil, V. V. Kulkarni, T. D. Dongale and S. A. Jadhav, *J. Compos. Sci.*, 2023, **7**, 167.
45 R. Yang, Y. Fan, R. Ye, Y. Tang, X. Cao, Z. Yin and Z. Zeng, *Adv. Mater.*, 2021, **33**, 2004862.
46 X. Liao, C. Pana, Y. Pana and C. Yin, *J. Alloys Compd.*, 2021, **888**, 161619.
47 S. Pundir, S. Upadhyay, R. Priya, N. Kumar, S. Chetana, I. Hossain, N. C. Joshi and O. P. Pandey, *J. Solid State Electrochem.*, 2023, **27**, 531–538.
48 Y. Zhu, H. Xu, P. Chen, Y. Bao, X. Jiang and Y. Chen, *Electrochim. Acta*, 2022, **413**, 140146.
49 J. M. O. Cremonezzi, D. Y. Tiba and S. H. Domingues, *SN Appl. Sci.*, 2020, **2**, 1689.
50 M. Jayachandran, A. Rose, T. Maiyalagan, N. Poongodi and T. Vijayakumar, *Electrochim. Acta*, 2021, **366**, 137412.
51 M. Moniruzzaman, Y. Anil Kumar, M. R. Pallavolu, H. M. Arbi, S. Alzahmi and I. M. Obaidat, *Nanomaterials*, 2022, **12**, 3187.
52 C. Deng, Z. He, J. Huang, L. Liu, Y. Liu, T. Wang, G. Chen, Y. Yi and K. Du, *Appl. Surf. Sci.*, 2023, **627**, 157299.
53 X. Dai, M. Zhang, T. Li, X. Cui, Y. Shi, X. Zhu, P. Wangyang, D. Yang and J. Li, *Vacuum*, 2022, **195**, 110692.
54 J. Wu, W. Raza, P. Wang, A. Hussain, Y. Ding, J. Yu, Y. Wu and J. Zhao, *Electrochim. Acta*, 2022, **418**, 140339.
55 S. Saini, P. Chand and A. Joshi, *J. Energy Storage*, 2023, **71**, 108209.
56 Z. Zhai, L. Zhang, T. Du, B. Ren, Y. Xu, S. Wang, J. Miao and Z. Liu, *Mater. Des.*, 2022, **221**, 111017.
57 J. Zhou, S. Zhang, Y. N. Zhou, W. Tang, J. Yang, C. Peng and Z. Guo, *Electrochem. Energy Rev.*, 2021, **4**, 219–248.
58 Y. Chen, X. Guo, A. Liu, H. Zhu and T. Ma, *Sustainable Energy Fuels*, 2021, **5**, 3017–3038.
59 A. Shetty, V. Molahalli, A. Sharma and G. Hegde, *Catalysts*, 2022, **13**, 20.
60 Y. Liu, J. Chen, B. Cui, P. Yin and C. Zhang, *C*, 2018, **4**, 53.
61 H. Yang, S. Ye, J. Zhou and T. Liang, *Front. Chem.*, 2019, **7**, 274.
62 H. Lu and X. S. Zhao, *Sustainable Energy Fuels*, 2017, **1**, 1265–1281.
63 J. Wang, X. Zhang, Z. Li, Y. Ma and L. Ma, *J. Power Sources*, 2020, **451**, 227794.
64 Z. Pan, S. Yu, L. Wang, C. Li, F. Meng, N. Wang, S. Zhou, Y. Xiong, Z. Wang, Y. Wu, X. Liu, B. Fang and Y. Zhang, *Nanomaterials*, 2023, **13**, 1744.
65 A. Mariappan, R. K. Dharman, T. H. Oh, S. Prabu and K.-Y. Chiang, *Mater. Chem. Phys.*, 2023, **309**, 128321.
66 D. Sui, M. Yao, L. Si, K. Yan, J. Shi, J. Wang, C. C. Xu and Y. Zhang, *Carbon*, 2023, **205**, 510–518.
67 Q. Ding, M. Zhang and H. Huang, *Mater. Lett.*, 2023, **333**, 133675.
68 Y. Jin, W. Tang, J. Wang, F. Ren, Z. Chen, Z. Sun and P.-G. Ren, *J. Alloys Compd.*, 2023, **932**, 167627.
69 H. Wang, H. Chen, C. Chen, M. Li, Y. Xie, X. Zhang, X. Wu, Q. Zhang and C. Lu, *Chin. Chem. Lett.*, 2023, **34**, 107465.
70 Z. Zhang, S. Lu, Y. Li, J. Song, E. Han, H. Wang and Y. He, *Ind. Crops Prod.*, 2023, **203**, 117155.

71 R. Wang, X. Li, Z. Nie, Q. Jing, Y. Zhao, H. Song and H. Wang, *J. Energy Storage*, 2022, **51**, 104364.
72 Y. Yao, T. Xie, P. Li, W. Du, J. Jiang, H. Ding, T. Zhao, G. Xu and L. Zhang, *Diamond Relat. Mater.*, 2023, **138**, 110169.
73 A. Agrawal, A. Gaur and A. Kumar, *J. Energy Storage*, 2023, **66**, 107395.
74 R. Mehdi, S. R. Naqvi, A. H. Khoja and R. Hussain, *Fuel*, 2023, **348**, 128529.
75 W. Tian, P. Ren, J. Wang, X. Hou, A. Sun, Y. Jin and Z. Chen, *J. Energy Storage*, 2023, **63**, 107039.
76 G. Li, Y. Li, X. Chen, X. Hou, H. Lin and L. Jia, *J. Colloid Interface Sci.*, 2022, **605**, 71–81.
77 D. J. Tarimo, K. O. Oyedotun, N. F. Sylla, A. A. Mirghni, N. M. Ndiaye and N. Manyala, *J. Energy Storage*, 2022, **51**, 104378.
78 D. Li, Y. Huang, C. Yu, C. Tang and J. Lin, *Diamond Relat. Mater.*, 2023, **136**, 109956.
79 M. Zhou, P. Wang, Y. Yu, W. Ma, Z. Cai, F. Ko, M. Li and Q. Wang, *Energy*, 2023, **278**, 127705.
80 Z. Zhang, S. Lu, Y. Li, J. Song, E. Han, H. Wang and Y. He, *Ind. Crops Prod.*, 2023, **203**, 117155.
81 S. Cheng, X. Wang, K. Du, Y. Mao, Y. Han, L. Li, X. Liu and G. Wen, *Molecules*, 2023, **28**, 5020.
82 A. T. S. C. Brandão, S. State, R. Costa, P. Potorac, J. A. Vázquez, J. Valcarcel, A. F. Silva, L. Anicai, M. Enachescu and C. M. Pereira, *ACS Omega*, 2023, **8**, 18782–18798.
83 A. Singh and A. K. Ojha, *J. Mater. Sci.: Mater. Electron.*, 2023, **34**, 1003.
84 T. E. Kibona, D. J. Mahushi and G. N. Shao, *Biofuels, Bioprod. Biorefin.*, 2023, bbb.2523.
85 H. Rustamaji, T. Prakoso, H. Devianto, P. Widiatmoko and W. H. Saputera, *J. Energy Storage*, 2022, **52**, 104724.
86 V. Raghavan and S. J. Rajasekaran, *J. Electrochem. Sci. Eng.*, 2022, **12**, 545–556.
87 R. Zou, B. Wang, L. Zhu, L. Yan, F. Shi, Y. Sun, B. Shao, S. Zhang and W. Sun, *Diamond Relat. Mater.*, 2022, **126**, 109060.
88 H. A. Hamouda, H. I. Abdu, Q. Hu, M. A. Abubaker, H. Lei, S. Cui, A. I. Alduma, H. Peng, G. Ma and Z. Lei, *Front. Chem.*, 2022, **10**, 1024047.
89 E. Elanthamilan, S. J. Jennifer, S.-F. Wang and J. P. Merlin, *Mater. Chem. Phys.*, 2022, **286**, 126188.
90 A. R. Selvaraj, D. Chinnadurai, I. Cho, J.-S. Bak and K. Prabakar, *J. Energy Storage*, 2022, **52**, 104928.
91 V. S. Bhat, A. Toghan, G. Hegde and R. S. Varma, *J. Energy Storage*, 2022, **52**, 104776.
92 G. Qiu, Z. Miao, Y. Guo, J. Xu, W. Jia, Y. Zhang, F. Guo and J. Wu, *Colloids Surf., A*, 2022, **650**, 129575.
93 M. Jalalah, S. Rudra, B. Aljafari, M. Irfan, S. S. Almasabi, T. Alsuwian, M. I. Khazi, A. K. Nayak and F. A. Harraz, *Electrochim. Acta*, 2022, **414**, 140205.
94 E. Gür, T. G. Semerci and F. Semerci, *J. Energy Storage*, 2022, **51**, 104363.
95 K. Li, J. Luo, M. Wei, X. Yao, Q. Feng, X. Ma and Z. Liu, *Diamond Relat. Mater.*, 2022, **127**, 109196.
96 E. Taer, N. Y. Effendi, R. Taslim and A. Apriwandi, *J. Mater. Res. Technol.*, 2022, **19**, 4721–4732.
97 K. Subhani, X. Jin, N. Hameed, A. K. Lau, J. A. M. Ramshaw, V. Glattauer and N. V. Salim, *Mater. Today Sustain.*, 2022, **18**, 100152.
98 F. Wu, X. Ren, F. Tian, G. Han, J. Sheng, Y. Yu, Y. Liu and W. Yang, *New J. Chem.*, 2022, **46**, 19667–19674.
99 Y. Liu, X. Cheng and S. Zhang, *Carbon Lett.*, 2022, **32**, 251–263.
100 W. Hu, B. Wang, Y. Yu, N. Wang and X. Wu, *J. Alloys Compd.*, 2021, **884**, 161149.
101 Y. Yin, S. Yan, Z. Ni, C. Jin and L. Zhao, *Biomass Convers. Biorefin.*, 2023, **13**, 12115–12124.
102 P. H. Patil, S. B. Ravan, S. S. Thoravat, T. D. Dongale and S. A. Jadhav, *Korean J. Chem. Eng.*, 2023, **40**, 2087–2090.
103 J. R. Choudhuri, S. P. Singh, A. K. Agarwal, K. Kumar and S. K. Srivastav, *Metal oxide-carbon nanocomposites for electrochemical storage*, Springer Nature Singapore, 2022, pp. 49–67.
104 S. S. Thoravat, V. S. Patil, S. S. Kundale, T. D. Dongale, P. S. Patil and S. A. Jadhav, *Synth. Met.*, 2023, **294**, 117312.
105 M. Bilal, Z. U. Rehman, J. Hou, S. Ali, S. Ullah and J. Ahmad, *Metal oxide carbon composite: Synthesis and properties by using conventional enabling technologies*, Elsevier, 2022, pp. 25–60.
106 J. R. Choi, J. W. Lee, G. Yang, Y.-J. Heo and S.-J. Park, *Catalysts*, 2020, **10**, 256.
107 D. Ma, X. Mu, G. Zhao, X. Qin and M. Qi, *Coatings*, 2023, **13**, 707.
108 T. Huang, C. Zhao, L. Wu, X. Lang, K. Liu and Z. Hu, *Ceram. Int.*, 2017, **43**, 1968–1974.
109 T. Bi, H. Chen, J. Li, X. Zhang and Q. Lin, *Electrochim. Acta*, 2022, **433**, 141266.
110 S. Saini, P. Chand and A. Joshi, *J. Energy Storage*, 2021, **39**, 102646.
111 J. Zhang, H. Chen, J. Bai, M. Xu, C. Luo, L. Yang, L. Bai, D. Wei, W. Wang and H. Yang, *J. Alloys Compd.*, 2021, **854**, 157207.
112 G. Lin, R. Ma, Y. Zhou, Q. Liu, X. Dong and J. Wang, *Electrochim. Acta*, 2018, **261**, 49–57.
113 J. Li, Y. Zou, C. Xiang, F. Xu, L. Sun, B. Li and J. Zhang, *J. Energy Storage*, 2021, **42**, 103017.
114 K. Cong, M. Radtke, S. Stumpf, B. Schröter, D. G. G. McMillan, M. Rettenmayr and A. Ignaszak, *Mater. Renew. Sustain. Energy*, 2015, **4**, 5.
115 S. Gao, Y. Chen, H. Fan, X. Wei, C. Hu, H. Luo and L. Qu, *J. Mater. Chem. A*, 2014, **2**, 3317.
116 A. J. Christina Mary, C. I. Sathish, P. S. Murphin Kumar, A. Vinu and A. C. Bose, *Electrochim. Acta*, 2020, **342**, 136062.
117 D. Bejjanki, P. Banothu, V. B. Kumar and P. S. Kumar, *C*, 2023, **9**, 24.
118 J. Bu, Z. Zhou, X. Wu, C. Zhang and Z. Li, *J. Mater. Sci.*, 2021, **56**, 17694–17708.
119 Z. Li, R. Wang, R. Zhong, A. Zhou, X. Wang and Z. Yang, *J. Mater. Sci.: Mater. Electron.*, 2022, **33**, 1899–1909.
120 Z. Sui, Z. Chang, X. Xu, Y. Li, X. Zhu, C. Zhao and Q. Chen, *Diamond Relat. Mater.*, 2020, **108**, 107988.
121 B. Sun, X. Zhang, X. Fan, R. Wang, H. Bai and X. Wei, *Energy*, 2022, **249**, 123659.

122 T. Kongthong, C. Poochai, C. Sriprachuabwong, A. Tuantranont, S. Nanan, N. Meethong, P. Pakawatpanurut, T. Amornsakchai and J. Sodtipinta, *J. Sci.: Adv. Mater. Devices*, 2022, **7**, 100434.
123 D. Li, J. Lin, Y. Lu, Y. Huang, X. He, C. Yu, J. Zhang and C. Tang, *J. Alloys Compd.*, 2020, **815**, 152344.
124 Y. Wang, J. Wang, D. Wei and L. Xu, *J. Colloid Interface Sci.*, 2023, **648**, 925–939.
125 *Handbook of Nanocomposite Supercapacitor Materials II: Performance*, ed. K. K. Kar, Springer International Publishing, Cham, 2020, vol. 302.
126 J.-W. Wang, Y. Chen and B.-Z. Chen, *J. Electrochem. Soc.*, 2015, **162**, A1654–A1661.
127 Y. Liu, S. Zuo, B. Shen, Y. Wang and H. Xia, *Int. J. Electrochem. Sci.*, 2020, **15**, 7646–7662.
128 S. He and W. Chen, *J. Power Sources*, 2015, **294**, 150–158.
129 H. Li, B. Wang, X. He, J. Xiao, H. Zhang, Q. Liu, J. Liu, J. Wang, L. Liu and P. Wang, *J. Mater. Chem. A*, 2015, **3**, 9754–9762.
130 C. Mao, S. Liu, L. Pang, Q. Sun, Y. Liu, M. Xu and Z. Lu, *RSC Adv.*, 2016, **6**, 5184–5191.
131 J. Chen, J. Qiu, B. Wang, H. Feng, Y. Yu and E. Sakai, *J. Electroanal. Chem.*, 2017, **791**, 159–166.
132 Q. Chen, J. Chen, Y. Zhou, C. Song, Q. Tian, J. Xu and C.-P. Wong, *Appl. Surf. Sci.*, 2018, **440**, 1027–1036.
133 S. Kong, B. Jin, X. Quan, G. Zhang, X. Guo, Q. Zhu, F. Yang, K. Cheng, G. Wang and D. Cao, *J. Electroanal. Chem.*, 2019, **850**, 113412.
134 C. Feng, D. Chen, Y. Tang, S. Chen, Y. Liu, C. Zhu, W. Xie, L. Ye, Q. Zhang, P. Qian, X. Feng, X. Dong and H. Jin, *Int. J. Electrochem. Sci.*, 2019, **14**, 8284–8295.
135 M. Li, J. Yu, X. Wang and Z. Yang, *Appl. Surf. Sci.*, 2020, **530**, 147230.
136 D. Li, J. Lin, Y. Lu, Y. Huang, X. He, C. Yu, J. Zhang and C. Tang, *J. Alloys Compd.*, 2020, **815**, 152344.
137 C. Li, X. Dong, Y. Zhang, J. Hu, W. Liu, X. Cui and A. Hao, *Appl. Surf. Sci.*, 2020, **527**, 146842.
138 J. Yu, M. Li, X. Wang and Z. Yang, *ACS Omega*, 2020, **5**, 16299–16306.
139 M. Yang, D. S. Kim, S. B. Hong, J.-W. Sim, J. Kim, S.-S. Kim and B. G. Choi, *Langmuir*, 2017, **33**, 5140–5147.
140 A. A. Mohammed, C. Chen and Z. Zhu, *J. Power Sources*, 2019, **417**, 1–13.
141 P. Zhang, Y. Wu, H. Sun, J. Zhao, Z. Cheng and X. Kang, *Int. J. Miner., Metall. Mater.*, 2021, **28**, 1735–1744.
142 H. Shen, X. Kong, P. Zhang, X. Song, H. Wang and Y. Zhang, *J. Alloys Compd.*, 2021, **853**, 157357.
143 S. Nirmaladevi, R. Boopathiraja, S. K. Kandasamy, S. Sathishkumar and M. Parthibavarman, *Surf. Interfaces*, 2021, **27**, 101548.
144 C. Yuan, H. Lin, H. Lu, E. Xing, Y. Zhang and B. Xie, *Appl. Energy*, 2016, **178**, 260–268.
145 X. Hu, W. Xiong, W. Wang, S. Qin, H. Cheng, Y. Zeng, B. Wang and Z. Zhu, *ACS Sustainable Chem. Eng.*, 2016, **4**, 1201–1211.
146 D. Deng, B.-S. Kim, M. Gopiraman and I. S. Kim, *RSC Adv.*, 2015, **5**, 81492–81498.
147 X. Yuan, Y. Zhang, Y. Yan, B. Wei, K. Qiao, B. Zhu, X. Cai and T.-W. Chou, *Chem. Eng. J.*, 2020, **393**, 121214.
148 Y. Li, N. Yu, P. Yan, Y. Li, X. Zhou, S. Chen, G. Wang, T. Wei and Z. Fan, *J. Power Sources*, 2015, **300**, 309–317.
149 J. Wang, H. Yang, Q. Sun, C. Zhou, X. Zhang, L. Ge and X. Ma, *Mater. Lett.*, 2021, **285**, 129116.
150 Q. Lu, S. Zhou, M. Cheng, B. Li, H. Wei, L. Zhang, Y. Zhang, J. Zhao, J. Zhang and Q. Liu, *Electrochim. Acta*, 2020, **363**, 137240.
151 Y. Tan, C. Yang, W. Qian and C. Teng, *J. Alloys Compd.*, 2020, **826**, 154133.
152 X.-S. Li, M.-M. Xu, Y. Yang, Q.-B. Huang, X.-Y. Wang, J.-L. Ren and X.-H. Wang, *Materials*, 2019, **12**, 2379.
153 T. Yu, F. Wang, X. Zhang, G. Lv, H. Lv, J. Wang, Y. Zhai and M. Li, *Diamond Relat. Mater.*, 2021, **116**, 108450.
154 P. Konnerth, D. Jung, J. W. Straten, K. Raffelt and A. Kruse, *Mater. Sci. Energy Technol.*, 2021, **4**, 69–80.
155 R. R. Palem, S. Ramesh, C. Bathula, V. Kakani, G. D. Saratale, H. M. Yadav, J.-H. Kim, H. S. Kim and S.-H. Lee, *Ceram. Int.*, 2021, **47**, 26738–26747.
156 Y. Wen, T. Qin, Z. Wang, X. Jiang, S. Peng, J. Zhang, J. Hou, F. Huang, D. He and G. Cao, *J. Alloys Compd.*, 2017, **699**, 126–135.
157 L. Wang, Y. Zheng, S. Chen, Y. Ye, F. Xu, H. Tan, Z. Li, H. Hou and Y. Song, *Electrochim. Acta*, 2014, **135**, 380–387.
158 G. Yang and S.-J. Park, *J. Alloys Compd.*, 2018, **741**, 360–367.
159 C. Wang, Y. Xiong, H. Wang and Q. Sun, *J. Colloid Interface Sci.*, 2018, **528**, 349–359.
160 B. Liu, Y. Liu, H. Chen, M. Yang and H. Li, *ACS Sustainable Chem. Eng.*, 2019, **7**, 3101–3110.
161 Y. Ping, Z. Liu, J. Li, J. Han, Y. Yang, B. Xiong, P. Fang and C. He, *J. Alloys Compd.*, 2019, **805**, 822–830.
162 T. Yumak, G. A. Yakaboylu, O. Oginni, K. Singh, E. Ciftyurek and E. M. Sabolsky, *Colloids Surf., A*, 2020, **586**, 124150.
163 X. Du, C. Hou, H. Kimura, X. Xie, H. Jiang, X. Sun, X. Yang, Y. Zhang and W. Du, *J. Energy Storage*, 2023, **72**, 108355.
164 A. Ganesh, T. Sivakumar and G. Sankar, *J. Mater. Sci.: Mater. Electron.*, 2022, **33**, 14772–14783.
165 Z. Wang, S. Wen, J. Ma, Z. Li, J. Wang and X. Liu, *Diamond Relat. Mater.*, 2023, 110451.
166 P. Sengodan, R. Govindan, G. Arumugam, B. Chettiannan, M. Navaneethan, M. R. Pallavolu, M. Hussien, M. Selvaraj and R. Rajendran, *J. Energy Storage*, 2022, **50**, 104625.
167 X. Wang, J. Chu, H. J. Yan and H. K. Zhang, *Heliyon*, 2022, **8**, e10631.
168 L. Chen, F. Wang, Z. Tian, H. Guo, C. Cai, Q. Wu, H. Du, K. Liu, Z. Hao, S. He, G. Duan and S. Jiang, *Small*, 2022, **18**, 2201307.
169 S. Dhinesh, M. Priyadharshini, T. Pazhanivel and R. Gobi, *Mater. Technol.*, 2022, **37**, 1837–1845.
170 T. Kongthong, C. Poochai, C. Sriprachuabwong, A. Tuantranont, S. Nanan, N. Meethong, P. Pakawatpanurut,

T. Amornsakchai and J. Sodtipinta, *J. Sci.: Adv. Mater. Devices*, 2022, **7**, 100434.
171 T. Niu, R. Lou, Q. Cao, Y. Zhang, Y. Zhang, G. Wei and Z. Wang, *Mater. Chem. Phys.*, 2023, **305**, 127941.
172 J. Zhang, X. Du, H. Kimura, C. Hou, X. Sun, X. Yang, Y. Zhang, X. Xie and W. Du, *Appl. Surf. Sci.*, 2023, **623**, 157095.
173 V. Babaahmadi, S. E. M. Pourhosseini, O. Norouzi and H. R. Naderi, *Nanomaterials*, 2023, **13**, 1866.
174 P. Li, J. Wu, L. Tang, H. Liu, Y. Xu and D. Zhang, *Ionics*, 2023, **29**, 3629–3639.
175 L. Wang, X. Wang, J. Ouyang, Y. Guo, W. Xiong, L. Zhao, M. Li, Z. Hua, Z. Li, K. Du, C. Zhou and Y. Luo, *Appl. Surf. Sci.*, 2023, **612**, 155821.